RADC-TR-81-292
Final Technical Report
October 1981

SURFACE MODIFICATION IN CONTROL SiO_2 FIBER FRACTURE

Massachusetts Institute of Technology

Roy Kaplow

ROME AIR DEVELOPMENT CENTER
Air Force Systems Command
Griffiss Air Force Base, New York 13441

This report has been reviewed by the RADC Public Affairs Office (PA) and is releasable to the National Technical Information Service (NTIS). At NTIS it will be releasable to the general public, including foreign nations.

RADC-TR-81-292 has been reviewed and is approved for publication.

APPROVED: John K. Kennedy

JOHN K. KENNEDY, Chief
EM Materials Technology Branch
Solid State Sciences Division

APPROVED: Freeman D. Shepherd

FREEMAN D. SHEPHERD
Acting Director
Solid State Sciences Division

FOR THE COMMANDER: John P. Huss

JOHN P. HUSS
Acting Chief, Plans Office

If your address has changed or if you wish to be removed from the RADC mailing list, or if the addressee is no longer employed by your organization, please notify RADC (ESM) Hanscom AFB MA 01731. This will assist us in maintaining a current mailing list.

Do not return copies of this report unless contractual obligations or notices on a specific document requires that it be returned.

UNCLASSIFIED

SECURITY CLASSIFICATION OF THIS PAGE (When Data Entered)

REPORT DOCUMENTATION PAGE		READ INSTRUCTIONS BEFORE COMPLETING FORM
1. REPORT NUMBER RADC-TR-81-292	2. GOVT ACCESSION NO. AD-A108796	3. RECIPIENT'S CATALOG NUMBER
4. TITLE (and Subtitle) SURFACE MODIFICATION IN CONTROL SiO_2 FIBER FRACTURE		5. TYPE OF REPORT & PERIOD COVERED Final Technical Report 22 Feb 79 - 22 Feb 81
		6. PERFORMING ORG. REPORT NUMBER N/A
7. AUTHOR(s) Roy Kaplow		8. CONTRACT OR GRANT NUMBER(s) F19628-79-C-0055
9. PERFORMING ORGANIZATION NAME AND ADDRESS Department of Materials Science & Engineering Massachusetts Institute of Technology Cambridge MA 02139		10. PROGRAM ELEMENT, PROJECT, TASK AREA & WORK UNIT NUMBERS 62702F 46001728
11. CONTROLLING OFFICE NAME AND ADDRESS Deputy for Electronic Technology (RADC/ESM) Hanscom AFB MA 01731		12. REPORT DATE October 1981
		13. NUMBER OF PAGES 150
14. MONITORING AGENCY NAME & ADDRESS(if different from Controlling Office) Same		15. SECURITY CLASS. (of this report) UNCLASSIFIED
		15a. DECLASSIFICATION/DOWNGRADING SCHEDULE N/A

16. DISTRIBUTION STATEMENT (of this Report)

Approved for public release; distribution unlimited.

17. DISTRIBUTION STATEMENT (of the abstract entered in Block 20, if different from Report)

Same

18. SUPPLEMENTARY NOTES

RADC Project Engineer: Martin G. Drexhage (ESM)

19. KEY WORDS (Continue on reverse side if necessary and identify by block number)

Hydrolyzing Siloxane Bonds
Carborizing
Tensile Strength
Dipole Layer

20. ABSTRACT (Continue on reverse side if necessary and identify by block number)

It is known that corrosion resistance can be imparted to various materials by carefully controlling the chemical environment to which newly formed and atomically clean surfaces are initially exposed. We take the view that the embrittlement of silica (SiO_2) is also a corrosion process, originating from the activated hydrolysis of siloxane (Si-O-Si) bonds by molecular water. Our approach considers that surface states of SiO_2 can be altered by the presence of absorbed or chemisorbed gases so as to

DD FORM 1 JAN 73 1473 EDITION OF 1 NOV 65 IS OBSOLETE

UNCLASSIFIED

SECURITY CLASSIFICATION OF THIS PAGE (When Data Entered)

increase the activation energy required for the absorption of water vapor or alternatively to impede the dissociation of molecular water on silica surfaces. Either of these mechanisms should raise the activation energy involved in hydrolyzing siloxane bonds and thus lower the susceptibility for crack propagation.

Gases containing straight or branched chain hydrocarbons are expected to reduce the absorption potential for H_2O for the silics surface. Absorbed gases containing strong polar residues such as halogens are expected to establish a surface dipole layer which may repel the absorbing end of H_2O and prevent its dissociation on the silica surface.

Crack free and atomically clean silica surfaces were prepared in ultra high vacuum (UHV) by electron beam evaporation from a high purity source and deposited on molybdenum foil as a film up to 5 micron thick. They were exposed to various experimental gases both before and after annealing and subsequently strength tested in ambient by a fracture-bend device which allowed testing of the tensile strength of the film on its substrate. The yield stress statistics for samples receiving exposure to different gases were found to be comparable to those of untreated controls and to the yield stresses of silica films receiving metallic coatings, thus indicating that stress corrosion was not the strength limiting process occurring in these samples. A group of samples which were found to be virtually crack free and in which stress corrosion was demonstrated to be the strength controlling process was prepared from cladded predawn fibers by carborizing the plastic cladding just before treatment. Their surfaces were not atomically clean, but they could be dehydrated by heating under vacuum to produce a moderately reactive surface consisting of free and hydrogen bonded silanol groups. Ammonia catalyzed condensation of N-butanol at the free surface silanols produced a hydrophobic layer of butyl-silyl groups. The layer did not significantly increase the yield stress of the fibers over control.

Successful surface modification was not achieved in these studies. The demonstration of tensile strength enhancement will require producing silica structures in which not only is stress corrosion the strength limiting process but also which contain a high density of unsaturated Si^+ and O^- reactive groups which can combine with selected gases to produce a layer with few coating flaws. Such test structures can probably be best prepared from declad drawn fibers by sputtering away surface contaminants or by heating the fibers to temperatures close to melting in UHV.

TABLE OF CONTENTS

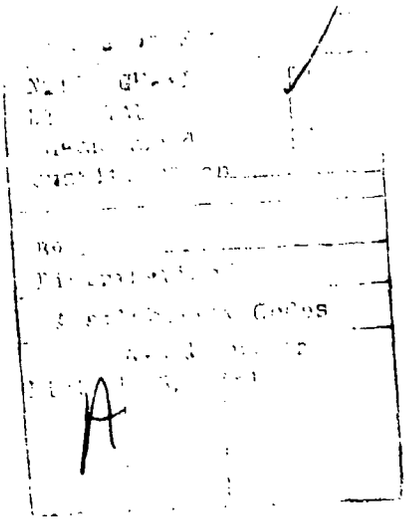

1. INTRODUCTION

1.1 Purpose of Study

This project relates to the establishment of procedures to apply to the manufacture of drawn optical fibers to improve their fracture strength. Most optical fibers currently in service have a composition that varies continuously from a core of mixed GeO_2 - SiO_2 composition to an outside shell of pure SiO_2. Currently, the fibers are coated with a plastic or metallic film as soon as they are drawn to protect the surfaces from attack by atmospheric gases, which otherwise reduces their tensile strength. The purpose of this study is to investigate the action of various gases, or combination of gases, which when adsorbed on a clean silica surface, reduces or prevents the weakening of bulk SiO_2 as normally occurs on exposure to atmospheric gases.

1.2 Brittle Fracture

The fracture strength of silica glass is usually much less than would be predicted from the interatomic bond energy. In glasses, brittle fracture occurs by the formation and propagation of a crack. When a crack is formed under an applied tensile stress, the stress on the material close to the crack tip is much greater than the average stress over

the whole cross section. The critical value of tensile stress required to hold an elastic crack at a given length was first calculated by Griffith [1]. In modern approaches, the criterion for crack arrest is developed in terms of a stress intensity factor evaluated at a short distance ahead of the crack tip [2].

1.3 Stress Corrosion

It is probable that the atmospheric corrosion of silicate glasses is caused and controlled by a chemical reaction between water in the environment and the glass [3]. The corrosion process is particularly accelerated under conditions in which the glass is under stress. The activation energy required for the chemisorption of water could derive from the surface energy of the glass and the reaction would be expected to occur most rapidly where the stress fields were the greatest. This rationale led Hillig and Charles [4], to conclude that water ought to react most rapidly at the crack tip, severing Si-O bonds and extending the crack length until the Griffith conditions for failure are satisfied. They developed these ideas into a quantitative theory for static fatigue; their expression for crack velocity, expressed in terms of an interfacial surface energy between the glass and the reaction products, has been partially verified experimentally.

Static fatigue was found to depend on the temperature of the test environment and did not occur at 77°K. At higher temperatures, the delayed time to failure obeyed an Arhenius type of equation, with an activation energy of 18.8 Kcal/mole [5].

1.4 Approach of Study

The approach we take is that surface states of SiO_2 can be altered by the presence of adsorbed or chemisorbed gases so as to increase the activation energy involved in hydrolyzing surface bonds. The effect would be to lower the susceptibility for crack propagation. The coupling of permanent molecular multipole moments of the selected adsorbate molecules with the electric fields at the silica surface can give rise to significant changes in the heats of adsorption of water vapor [6,7] and in the activation energy required for hydrolysis. Westwood and Huntington [8] found evidence that the attachment of long chain alcohols to the surface of soda lime glass would produce more than a factor of two variations in the effective surface energy required to produce a given crack velocity when measured in the liquid alcohol as the chain length of the alcohol is varied. Much of their evidence points towards a mechanism involving surface electrical charge and the resulting electric field effect on point defect concentration and ionic mobility.

To guarantee accessibility of the gases or liquid vapors known or suspected of adsorbing to the silica surface, we prepare atomically clean, pristine silica surfaces in ultra high vacuum (UHV). These conditions assure us of adequate controls over surface contamination both prior to and during the administration of potential passivating gases. In addition, the preparation of samples in UHV allows us to control the hydroxyl content of the surface, which presumably is rapidly established when unsaturated Si^+ and O^- ions combine with water and oxygen in their surround, when the glass is pulled from the melt. In particular, UHV conditions should allow us to substitute other reactive groups for the normally found hydroxyl groups by saturating the dangling Si^+ and O^- bonds with selected gases.

1.5 Adsorption/Chemisorption to Surface Active Groups

The surface of drawn glass fibers in normal manufacture is hydrated by atmospheric water almost as soon as it is drawn. Some of this water can be removed by thermal treatment under vacuum to produce a reactive silanol group (see below) and some of it condenses to form a virtually unreactive siloxane group. In searching for a passivation treatment which will increase the heats of adsorption of water, as well as to raise the activation energy required for hydrolysis of the Si-O bond, one wants to start with as clean a silica surface

as possible, possessing a large surface density of unsaturated Si^+ and O^- bonds. To appraise the likelihood of success of any particular treatment, it is important to consider the chemical reactivity of the different silica surfaces which can be prepared and to consult the literature for information concerning the interactions with various gases.

1.5.1 Reactivity of Various Silica Surfaces

The nature of the surface interaction of silicate glasses with various gaseous reagents has been probed by gravimetric, thermodynamic, infra-red spectroscopic, and dielectric polarization techniques. Much of the work up to 1967 has been summarized in a review paper by Steele [7]. The properties of physically adsorbed gases have been modeled through consideration of the effects of hydration on the electric field at the silica surface. A dehydrated surface is essentially non-polar, being made up primarily of uncharged oxide groups. The heats of adsorption on such a surface are due either to inductive, dispersion interactions between the oxide atoms and the adsorbate molecules or the reaction of highly polar molecules with the oxide. The latter process accounts for the chemisorption of water and methanol on dehydrated silica and may be represented by

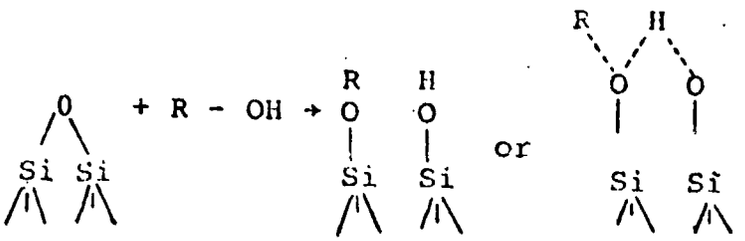

(1)

where R is any reactive group. Greenler [9] reported that methanol and ethanol were partly chemisorbed by reaction with surface oxides to form hydroxyls and methoxide or ethoxide groups at room temperature, with the formation of formate or acetate groups at higher temperatures. Surface esterification has also been reported by Dzhigit et al [10] and Belyakova and Kiselev [11].

The hydrated silica surface consists of polar hydroxyl groups (or hydrogen bonded protons). Ammonia, alcohols and similar polar gases form hydrogen bonds to the surface hydroxyls. These reactions can be represented by

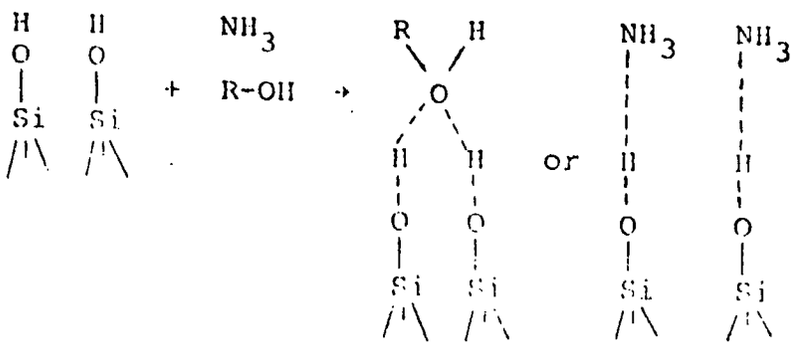

Non-polar hydrocarbons may also adsorb to surface hydroxyl groups via the π electron quadrupole-dipole interaction or charge transfer between an aromatic π system to an antibonding orbital of the surface hydroxyl [12]. Some of the gases whose adsorption is enhanced by increasing the content of surface hydroxyls are N_2 [13], ammonia (NH_3) [14], t-butyl alcohol [15], isobutanol [16], ethyl ether [17], benzene [18], butene [19], ethyl and methyl chloride [20], and substituted silanes including trimethl chlorosilane [6], dichlorodimethylsilane [21], vinyl trichlorosilane [22], and hexamethyldisilazane [23].

Of the number of citations found dealing with the reactivity of various gases, most studies examined initially hydrated silica surfaces which were partially dehydrated by thermal treatment to produce a moderately reactive, yet still contaminated surface. Such surfaces have been used to study the adsorption/desorption of water vapor. These studies are important to us because they determine the primary sites and the energetics for water adsorption on fibers which is the prerequisite event in the stress corrosion. The understanding is crucial in the design of gaseous treatments which will prevent its occurrence.

1.5.2 Water-Silica Interfaces

Infrared gravimetric adsorption data show that the major water adsorption sites on partially hydrophobic silicas are surface hydroxyl groups, which may be either freely vibrating or hydrogen bonded to each other, according as to whether surface silanols are vicinal to a siloxane or to another silanol, respectively [21]. At low surface water coverage (submonolayer and monolayer) the free silanols provide the donor hydrogen bond to the adsorbing water molecules [24]. The activation energy at less than monolayer coverages can be as low as 10 kcal/mole [25].

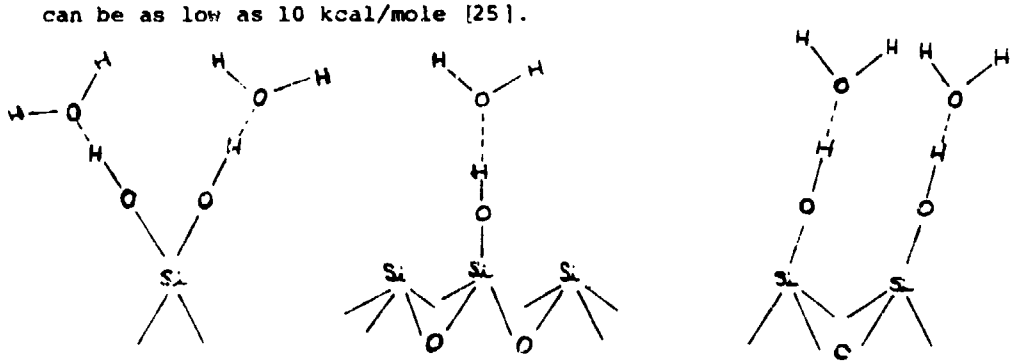

Geminal Hydroxyls | Freely Vibrating Hydroxyl | Vicinal Hydroxyls

Geminal OH groups (= Si $(OH)_2$) are probably not hydrogen bonded to their partners because a five or six membered ring is normally needed for intramolecular H bonding [26]. Water will adsorb preferentially on hydrogen bonded hydroxyl groups

and tend to form clusters even before all adsorption centers are occupied. The energy of activation necessary for the removal of physically adsorbed water is 7-8 kcal/mole [25]. The suggestion that water may diffuse into the silica and form hydroxyl groups in the interior [27] does not seem to be supported by experimental evidence [24].

The concentration of hydrogen bonded hydroxyls can be varied by thermal pretreatment. When heated under vacuum, the silica surface first loses physisorbed water and then loses additional water via the condensation of adjacent hydroxyls. The condensation is reversible up to about 400°C; after 800°C the surface becomes hydrophobic and only the freely vibrating silanol group is observed in the IR spectrum [21].

1.5.3 Alcohol-Silica Interfaces

Gases possessing non-polar residues have been used to bind to surface silanol groups, and project the hydrophobic end outward from the surface, rendering it less reactive. Such gases include alcohol vapors and substituted silanes.

Alcohols can undergo condensation reactions with free silanol groups. In the presence of a Lewis base such as ammonia or an organic amine the condensation goes to

completion at room temperature [28], consuming all of the free silanol groups and producing a covalent linkage that is stable to heating at 250°C. The enhancement of alcohol activity by the Lewis base is thought to involve the formation of an electronegative oxygen (the alcohol hydroxyl) via the transfer of the alcohol proton to protonate the amine. The electropositive protonated amine removes the silanol hydroxyl to form water. Alkylation of approximately 80% of the surface hydroxyl groups will also occur upon heating the silica surface to 360°C in the presence of methanol vapor in equilibrium with its room temperature liquid [29].

1.5.4 Silica-Siloxane Interfaces

Substituted silane gases react specifically with the freely vibrating hydroxyl groups on silica surfaces to form a covalent linkage of the Si-O-Si type which is stable at high temperatures [30]. The activation energies for bond formation depend upon the particular substituent groups of the silane which is adsorbed. The four chlorosilanes $(CH_3)_n Si Cl_{4-n}$ (n = 0 to 3) have activation energies of 22 ± 2 kcal/mole [31], the methoxysilanes - $(CH_3O)_{4-n} Si (CH_3)_n$ (n = 0 to 3) of 30.6 kcal/mole [30], and hexamethyldisilazane - $(CH_3)_3 Si-N(H)-Si (CH_3)_3$ of 18.5 kcal/mole [32]. Hexamethyldisilazane is considerably

more reactive than the other silanes, chemisorbing at a rapid rate at 30°C, compared with 200°C for the methoxysilanes and 350°C for the chlorosilanes. Infrared spectroscopy showed that the di and trifunctional organosilanes are capable of replacing geminal surface hydroxyls by second order kinetics with respect to the number of surface sites. Physical adsorption decreases with increasing temperature, but such silanes as hexamethyldisalazane and trimethylsilydiemethylamine are capable of removing all free surface hydroxyls.

One study compared the adsorption of water vapor on untreated alumino borosilicate "E" glass fibers and fibers which had been drawn in an atmosphere of a representative trifunctional organochlorosilane - vinyltrichlorosilane (VTS) [33]. The affinity of the "E" glass fibers for water vapor was enhanced by the reaction with VTS; but the untreated E glass showed an increase in microscopic surface area upon water adsorption. Babkin and Kiselev [6], found that trimethylsilated silica exhibited a marked weakening of the adsorption potential for water vapor, adsorption occurring only at sites of coating defects, presumably hydrogen bond surface hydroxyls. Apparently these were not all removed by the pretreatment.

1.5.5 Silica-Halogen Interfaces

Just as surface silanol groups can react with various chlorosilanes, they will also react with a variety of other halogenated compounds. All surface hydroxyl groups may be replaced by Si-Cl by reaction with Cl_2 at 700-950°C or with CCl_4 at 350-600°C, although not with HCl [34]. Si-Cl groups also are reaction products formed on treatment with $AlCl_3$ [35] and with $SOCl_2$ [36]. The exposure of the surface silanol groups to BCl_3 vapors results in their replacement by $SiO\text{-}BCl_2$ groups. The remaining chlorine atoms can serve as sites for other replacement reactions [37].

In semiconductor applications, the thermal oxidation of silicon in the presence of oxygen and chlorine containing compounds such as C_2HCl_3 and CCl_4 yielded improved dielectric breakdown characteristics over SiO_2 films grown just in oxygen alone. The low field breakdown in the oxide film was attributed to the presence of physical defects such as oxide pinholes and electrical defects such as charged interface states. The improvement in chlorinated oxides was attributed to the removal of these defects by halogens in the oxide [38] and the suppression of stacking faults [39].

2. Experimental Methods

2.1 Preliminary Search for Adequate Sample Preparation Methods

The demonstration of enhanced tensile strength of silica by treatment with gaseous surface active reagents requires not only that test samples to receive passivation be produced or cleaned in UHV, but that they also be free of surface microcracks. The latter requirement places severe limits on the methods of sample preparation acceptable for this study.

Several sample preparation techniques, useful for surface spectroscopy, could not be used to make samples for tensile stress testing. The oxidation of polished silicon wafers by exposure to molecular oxygen at 1000°C or to a high energy ionized beam of O_2^+ would yield a reproducible coating of SiO_2 (up to 5000 Å), but would not permit fracture of the SiO_2 without fracturing the silicon. The generally lower fracture strength of silicon (0.64 KN/cm^2) makes it impossible to measure the strength of the silica [40]. One approach given serious consideration in the early phases of research was that of etching nude optical fibers or polished fused silica strips under UHV conditions by argon ion bombardment. The secondary surfaces, created by sputtering the outermost material, would certainly be free

of atmospheric contaminants, and also, presumably, of microcracks since the argon beam etches uniformly over the exposed surface. The difficulty of reproducibly etching crack free silica surfaces by these means became apparent after the ion beam was observed to deflect from its preset target due to surface charging of the test specimen. An experiment consisting of abrading the mirror zone of a fractured silica surface with .3μ Al_2O_3 abrasive produced the surface scratches shown in Fig. 1. These scratches were not removed by raster sputting with Argon for 1.5 hrs. with a 4 kv beam. Even if smaller cracks could be removed, it was clear that one could not assume that an area large enough for tensile stress testing could be uniformly etched.

A plane surface of silica was judged to be the ideal geometry for studying the effectiveness of the argon beam in etching away surface layers to produce a crack free secondary surface on a polished silica plate. Commercially polished plate silicas all have subsurface cracks, originating from the initial grinding operation, which are not removed by polishing. It is clear that to enhance the tensile strength of such polished silica plates, one has to be able to uniformly etch the surface layers to a depth of perhaps 0.1 to 0.5μ.

We did not attempt to sputter etch material from the surface of drawn fiber silica because of the difficulty we had in focusing the ion beam on a much larger target and because of the need to etch uniformly around the entire circumference of the fiber. It is clear that a special apparatus is required to mount the fiber in such a way that its circumference could be sputtered and its accumulated change neutralized. An obvious advantage of using the drawn fiber is that the depth of etching need be much less than that required for polished plates because the depth of crack penetration is shorter in fibers. Still the difficulty in handling the drawn fibers without mechanically damaging them either before or after the passivation trial made us opt for the preparation detailed below.

The method of sample preparation that was finally employed, which it seemed would be able to satisfy both the mechanical testing and the UHV requirements, was the electron beam evaporation of SiO_2 and its deposition as a film 3 to 5μ thick on a metallic substrate. The chemical composition of such surfaces was determined by scanning Auger spectroscopy. Elemental surface analysis was obtained by dividing the relative peak to peak amplitudes for the various Auger transitions by their respective atomic sensitivity factors. These, in turn, were calibrated for the different spectrometer

settings from samples of fused silica and other materials. The oxygen:silicon stoichiometry of deposited glass was consistently found to be 2:1 to within experimental error (5%).

2.1.1 Factors Affecting Film Density

Studies in the literature which evaluated the composition of silica films produced by electron beam evaporation had shown earlier that the deposits retained the stoichiometry of the starting silica as judged by the similarity of their optical absorption around 1093 cm^{-1} and that of thermally grown silicon dioxide on silicon [41]. Unannealed films, however, exhibited porosity and strain compared to the thermally grown films. Annealing at 980°C produced virtually the identical surface properties, judged by refractive index measurements, etch rates, and IR absorption spectra, as obtained for the thermally grown oxide [42]. Thermal oxidation of silicon has been studied with increasing oxygen coverages [43]. Above monolayer coverage both energy loss spectra and Auger spectra develop continuously into the spectra representative of SiO_2.

2.1.2 Sample Annealing

A ten strip substrate holder and annealing block, capable of reaching 1000°C quickly (for short testing cycles) was constructed and installed in a UHV chamber which was

specifically dedicated to the production of mechanical test samples. The substrate heater is a molybdenum block; insulated tungsten rods passing through the block carry up to 80 amperes of current to achieve the desired annealing temperature. The block temperature is measured with a platinum -10% rhodium thermocouple. The block is supported by two 0.635 cm diameter Mo shafts and can be rotated by 180° via external control, to expose either of the two major surfaces to the SiO_2 vapor stream; each side yields 5 sample strips. During annealing, the only conductive pathways for heat loss are two Mo vertical supports for the Mo shafts. The heater itself is nearly completely surrounded by a Mo radiation shield (Fig. 2).

Several refractory metals were tested for the use as substrates for silica deposition - Ni, Pd, Ta and Mo sheets varying in thickness from 0.000762 cm to 0.0127 cm. They were degreased in trichloroethylene and sonically washed in acetone, reagent methanol and ethyl ether, but were otherwise used as supplied by the manufacturer, except as specifically noted.

2.1.3 Unannealed Deposited Samples

SiO_2 samples were deposited onto substrates of nickel foil 0.00127 cm and 0.0127 cm thick which were held at 280°C.

In Table I we show the thickness, refractive index and composition values obtained for these samples. After deposition, the samples were exposed to an atmosphere of dry nitrogen in the vacuum chamber. Through and including this point, they appeared to remain free of fracture and well adhered to the substrates. Immediately upon exposure to ambient air (of relatively high humidity), however, the films on the substrates all cracked and most of the surfaces flaked off the substrates The films on the thinner substrates did not crack and remained adhered to their substrates.

We believe that these results can be interpreted in the following way. The evaporated films are under an internal stress. In the vacuum and in the dry nitrogen atmosphere, the film surfaces are able to withstand that stress. This is true even though -- for these unannealed samples -- the film bulk is extremely porous and the surface is largely covered with microscopic defects (pores). The immediate fractures, accompanied by much separation from the substrate, on presenting the samples to atmospheric air, is a dramatic manifestation of what we believe to be the corrosive effect of the moisture in the air. In this instance the fracture is then essentially spontaneous because of the residual internal stress in the films and the inherent film weakness because of the high porosity.

The fact that the films on the thin substrates did not fracture is likely due to the lower residual stresses in those films. Indeed, the thin substrates were found to be bent on removal; with the silica on the convex surface of the foil, indicating that the stresses in those SiO_2 films had been able to relax at least partially. On the other hand, we have found that the very thin substrates are less suitable for the subsequent mechanical tests and other characterizations. Fig. 3 shows a representative scanning electron micrograph of such an unannealed sample. The surface is seen to be covered with microscopic pores indicative of a lack of densification.

2.1.4 Annealed Deposited Samples

SiO_2 samples were deposited onto nickel foil 0.0127 cm thick and annealed at 1300°K. The samples were found to crack during the heating to the annealing temperature but were still otherwise adhering the substrate. In Table I, we list the physical characteristics measured for these samples as well as others deposited on Pd, Ta and Mo substrates.

The only silica films to always survive the heating and cooling cycle without cracking were those deposited on Mo substrates. Figs. (4, a,b,c,d) compare the surface morphologies of annealed and unannealed silica films which were deposited on

Mo substrates 0.0127 cm thick. The scanning micrographs show "pore-like" structures in the unannealed glass which are not evident in the annealed glass. The substrate temprature during deposition was the same in each case (T = 450°C), and the SiO_2 deposition rate was also identical.

The film density of SiO_2 has been related to its refractive index and to its acid etch rate [44]. We obtained the refractive indices of certain annealed and unannealed deposited films and compared them to the index of a plate of fused silica (Table I). Refractive index values were obtained through measurements of the plane of polarization of light reflected from the film surface, using a Gaertner ellipsometer. The data were analyzed with computer programs supplied by Hewlett-Packard as part of a thin film analysis laboratory computer software package using as input the film thickness as measured by a Sloan Dectac. There was not discernable difference between the refractive indices of annealed deposited films and that of the bulk fused silica sample.

2.2 Protocol for Passivation Treatment

In an effort to minimize internal stresses and to maximize the density of deposited films, the following protocol was adopted for the production of test samples. Silica is

deposited on a 0.0127 cm Mo foil substrate at 450°C by electron beam evaporation in a vacuum chamber whose base pressure is 10^{-9} torr. Film thickness is determined in situ with a vibrating quartz thickness monitor which is calibrated against direct measurements on deposited samples with a Sloan Dectac. The rate of deposition is manually maintained at approximately 750 Å/min. Silica is deposited to a thickness of about 4μ on substrates on both sides of the heating block and then annealed for 1 hr. at 1000°C. The time course for the rise and fall of the substrate temperature is about 10°C/minute. Substrate temperature, film thickness and vacuum pressure are plotted continuously during each run. The vacuum is at least 10^{-8} torr when the substrate is at 650°C or below and 10^{-6} torr when the substrate is at 1000°C. Fig. 5 is a photograph of the high vacuum system used to produce mechanical testing samples, showing some of the sample deposition and monitoring facilities.

2.3 Methods of Testing the Fracture Strength of Samples

Vacuum deposited glass films were measured for their tensile stress at fracture using either a three or four point bending test. The instrument to accomplish this was specially designed and constructed for these experiments to allow the measurement to be performed with the film adhering to the

substrate. Because of the high aspect ratio of the samples, the curvature is sufficiently large so that simple beam theory cannot be used.

Two rotating arms, driven by cams rotating in opposite directions about a single axis, bend the film and substrate around either a central knife edge (one point loading) or a double knife edge (two point loading) until fracture is observed in the glass under a microscope (Fig. 6 a,b). The angular velocity is a fixed 1.203 deg/sec. A manually operated electronic clutch stops the movement within 20 milliseconds after activation; this corresponds to an angular motion of 0.024 deg. An estimated operator response time of 0.5 sec. for crack recognition and clutch activation yields an angular error of 0.573 deg. This can be partially compensated for because it is systematic, but nonetheless dominates all other error sources in the bending cycle measurement. The angle of the bend (half of the included angle formed by the tangents to the sample surfaces) is read directly from a vernier scale. Angular resolution of the vernier is 0.05 deg.

The analysis of tensile stresses involved when samples undergo large deflections before they fracture is described in Appendix I. The situation is analogous to a beam simply

supported at its ends while loaded at one or two points. The theoretical framework is largely borrowed from the published literature, although certain corrections are made as well as specification to to the particular geometry we use. In addition, the analysis is expanded to consider the effective tensile stress in the outer fibers of a beam which is a composite of two different materials. The one point loading configuration has the advantage of having the simpler solution and is the one more commonly used for this study. The two point loading configuration introduces no shear forces on the center section of the beam, however, and while the analysis is more cumbersome from a theoretical standpoint, it is occasionally exploited because of its pure bending nature, to confirm the results of the one point loading test. All relationships between the included angle of bend (directly measured) and the theoretically relevant parameters of beam curvature were determined from photographic calibrations (Appendix I).

Test samples consisted of Mo substrates with deposited strips of silica having dimensions 0.653 cm x 5.08 cm x 0.003 to 0.0005 cm thick. Each strip would usually yield 3 to 5 data points. Approximately half of the available samples were tested as soon as possible after extraction from the vacuum chamber

and consequent exposure to atmospheric gases (within 40 min.). The remaining samples were tested after 24 hrs of incubation in an atmosphere of saturated water vapor at 25°C. Fracture statistics were calculated and plotted on frequency distribution versus yield stress axes on a Hewlett-Packard Model 85 microcomputer. Relevant programs appear in Appendix I.

2.4 Surface Cleaning of Standard, Predrawn Fibers

Standard, predrawn optical fibers as supplied by USAF RADC/ESM were coated with a 40μ thick plastic. This material was removed after the fibers were cut into 6 cm lengths and carbonized under electric heat for four or more hours until all visible carbon residues had oxidized completely. In experiments where fibers were used as test samples for the surface passivation trials, they were additionally cleaned by the following heat treatment under UHV conditions. They were carefully mounted on the top side of the Mo heating block by means of two .0254 cm thick shims, in contact with only the two ends of the fiber segment, leaving the center of the test section free of any contact abrasive surface. Under UHV conditions, the surface cleaning was accomplished by conductive and radiative heat transfer to the test section up to a sustained temperature of 400°C for several hours. Passivation experiments commenced at the elevated temperature, before the fibers had a chance to cool.

3. Results

3.1 Fracture Stresses for Comparative Standard Silicas

Fused silica fibers and plates were procured in order to test the reliability of the bending apparatus and to compare the fracture of vacuum prepared samples to those of commercially available fused silicas having similar shape and dimensions to the vacuum preparations. A 200μ diameter optical fiber received from USAF RADC/ESM was tested after the plastic cladding material was removed without abrading the glass by carbonizing under electric heat. The fracture statistics obtained from 40 samples within 40 minutes after removal of plastic (Fig. 7a) gave an average fracture stress of 82.92 ± 23.99 KN/cm^2. Fracture statistics obtained from samples after a 24 hr. incubation at 100% relative humidity (Fig. 7b) gave an average fracture stress of 100.46 ± 20.29 KN/cm^2. The higher yield stress here may be an indication that water has the ability to preferentially etch at the tip of a crack, making it rounder and less steep than before [45]. Yield stresses were also obtained on a sample of unclad fibers which were incubated in a water saturated atmosphere under a static, applied stress for 24 hrs. and then subjected to the bend test. The applied stress, less than that necessary to cause fracture, was administered by wrapping the fibers around a 9.843 cm diameter mandrel. The subsequent fracture tests

produced a lower mean yield stress of 68.38 $\pm$ 17.49 KN/cm^2 (Fig. 7c). This drop in fracture strength is a manifestation of the aforementioned static corrosion fatigue, and also a verification of the sensitivity of the bend-fracture device to changes in surface structure.

A significantly lower yield stress was found for thin Supersil$^{(R)}$ strips having the dimensions 0.635 cm x 5.08 cm x 0.025 cm which had been polished by the manufacturer (Amersil) to an optical finish with 0.05μ abrasive. During testing the compressive surface was covered with cellophane tape to enable identification of the site of crack initiation. Eighty percent of the samples showed that fracture initially occurred at an edge. The fracture statistics in Fig. 8a gave a mean tensile yield stress of 12.37 $\pm$ 1.76 KN/cm^2. Fracture statistics were also obtained on the same material after abrading the polished surface with 0.3μ $A\ell_2O_3$ abrasive. The abrading produced a higher fraction of cracks initiating from the polished surface (30%) but essentially the same yield stress as control ($\bar{\sigma}$ = 12.53 $\pm$ 1.87 KN/cm^2). When the polished surface was abraded by lightly scratching it with a diamond tip stylus to produce scratches of depth about 1μ, all fractures (100%) were initiated by surface cracks, rather than edge cracks; and the mean fracture strength dropped to

5.90 ± 1.13 KN/cm^2 (Fig. 8b). This, again, is a verification of the sensitivity of the bend-fracture device to changes in surface structure.

3.2 Unpassivated UHV Deposited Control Samples

Control test samples were prepared by vacuum deposition onto a Mo substrate 0.0127 cm thick to achieve a film thickness of between 3 to 5μ. Prior to use, the Mo substrate was degreased in trichloroethylene, and sonically washed in acetone, reagent methanol and ethyl ether, but was otherwise used as supplied. The mask used to outline sample area consisted of 5 rectangular slits 5.08 cm long and 0.635 cm wide. During deposition, the substrate temperature was maintained at 450°C. The film was annealed at 1300°K under a vacuum of 10^{-6} torr. (See Fig. 9 for the time course of heating and cooling). Annealing time varied between 20 min. and 1 hr. with no measurable difference in the fracture strength or surface morphology of the deposited films. Chamber pressure returned to 10^{-8} torr as substrate cooled to temperatures below 650°C. Samples were held overnight under vacuum, brought up to atmospheric pressure with N_2 and tested immediately after removal from the chamber. Total elapsed time between the first exposure to corrosive (ambient) gases and the time of test did not exceed 40 min.

Both three and four point bending tests were applied to these control samples. The four point tests were designed to check whether the shear forces introduced in the three point tests were causing premature failure of the glass. Figure 10 a,b shows the fracture statistics on these control samples. Mean fracture strength for the three point test was 8.46 $\pm$ 1.92 KN/cm^2. Mean fracture strength determined by the four point bending test was 8.12 $\pm$ 1.41 KN/cm^2. No cracks originated at an edge. All were confined to the central surface of the sample.

Additional control samples were allowed to incubate at 25°C in an atmosphere of 100% relative humidity for 24 hrs. prior to testing. Fracture stress statistics (Fig. 10c) from the three point bend test gave a mean value yield stress somewhat lower (7.80 $\pm$ 0.58 KN/cm^2) than the pre-exposure value; however, the greater standard deviation of the pre-exposure value was sufficient to make these differences insignificant.

The relatively low tensile stress tolerance of these control samples compared to the standard 200μ waveguide material was cause for concern. The control samples did compare favorably to the yield stresses obtained for the commercially polished fused silica rectangular strips of

comparable dimensions to the UHV samples. Scanning electron micrographs of the surface of control samples (Fig. 4, c,d) did not show the pore like features which were observable on the unannealed surfaces (Fig. 4 a,b). Ellipsometry measurements gave the index of refraction (1.46) appropriate for fused silica.

One source of the discrepancy in fracture strength between control and optical fiber samples may be associated with differences in the surface area under load. Assuming equal lengths of arc bearing the maximum tensile stresses in the two cases, the surface area under test for control was 20X the area under stress for the optical fiber. The path length around upper and under surfaces of control was 1.27 cm compared to a circumference of 0.063 cm for the 200μ fiber. This is analogous to testing optical fibers using different gauge lengths. Extrapolation of larger length (L_2) strength (σ_2) from shorter length (L_1) tests results (σ_1) at a particular failure probability is given by

$$\frac{\sigma_2}{\sigma_1} = \left(\frac{L_1}{L_2}\right)^{1/m}$$

(See Appendix II), where m is the exponent in the cumulative flaw distribution of Weibull [46]. For a typical value of m = 3 [47,48], the ratio of larger length strength to shorter length strength $\frac{\sigma_2}{\sigma_1} = 0.37$.

Some putative sources for the remaining discrepancy in fracture strengths of deposits and fiber include:

(a) residual stresses and flaws from film deposition

(b) stresses caused by the differential expansion of film and substrate on annealing

(c) surface roughness imparted to the film by the Mo substrate

(d) devitrification nuclei created on the under surface of the film during annealing.

In an effort to address the third possibility, commercial grade Mo thin sheets were either electropolished or hand polished down to 0.05μ grit abraisive. A photo etch quality Mo sheet (kindly supplied by Schwarzkopf Developnent Corporation) was also used as substrate. The differences in the surface roughness of these different preparations is made apparent

in the micrographs of Fig. 11 obtained with a polarizing light microscope. It was not possible to achieve a highly polished Mo surface either by hand or electropolishing methods. This is probably because the sheet is formed from compacted powders and sintered in hydrogen and has less than perfect density, since this material is difficult to work at temperatures below 600°C.

Silica films deposited on electropolished Mo substrates all cracked in the vacuum on increasing the temperature towards 1300°K, the usual annealing temperature. Silica films deposited on the hand polished Mo substrates withstood annealing as did those deposited on the photo etch quality Mo sheet and both appeared to be intact and well adhering.

The conspicuous frailty of deposits on electropolished Mo compared to the strength of deposits on untreated or hand polished Mo sheet did not seem to corroborate the suggestion that surface roughness of the substrate was influencing the fracture strength of the silica. Polarizing light micrographs showed that both electropolished and hand polished sheets have surface pits; these were larger and deeper in the case of the hand polished substrate (Fig. 11d), which nonetheless produced well formed films. Untreated, standard and photo etch quality sheets showed the highest density of surface pits and roll marks originating from their manufacture.

3.3 Fracture Stresses of Deposited Films with Amorphous and Polycrystalline Coatings

The literature reveals much evidence for the improvement of surface properties of silicate glasses by ceramic and polycrystalline coatings. Evaporated and sputtered oxides of vanadium and tantalum have been reported to protect glass against attack by alkalais [49]. The development of anti-reflective coatings for glass lenses produced surfaces which were hard wearing and water resistant. MgF_2 and CaF_2 films were found to be hard wearing when deposited on a hot glass surface (> 250°C) [50]. The critical temperature above which MgF_2 films undergo structural changes and became hard also coincides with that at which adsorbed water is effectively removed from glass surfaces at low pressures [51]. Above 100°C CaF_2 films were found to have a preferred orientation such that (111) planes of the crystals are parallel to the glass surface [52].

Two recent references in the patent literature claim to have formulated different types of coatings which protect silicate glasses against chemical corrosion; U.S. Patent 4,188,444 [53] describes a method which imparts al alkali resistant silicon coating to a glass surface. It

draws upon the published results of D.G. White and E.G. Rochow [54], that during the production of alkyl silanes by reaction of silane and ethylene or acetylene in a heated tube, a thin layer of silicon deposited on the inner surface of the heated tube. The presence of electron donating hydrocarbons is claimed to impart an alkali resistance to the silicon coating. The coating thickness is about 400 Å. U.S. Patent 4,118,211 [55] claims to maintain the mechanical strength of an optical fiber by coating the fiber with an inorganic ceramic material that is impervious to both moisture and chemically corrosive environments. The ceramic coating is applied immediately after the fiber is drawn by conventional chemical vapor deposition (CVD) techniques. Such ceramic materials include silicon nitride (Si_3N_4), boron nitride (BN), tin oxide (SnO_2) and titanium dioxide (TiO_2). The recommended thickness of the deposit is between 0.02 to 0.2μ. A silicon oxynitride ceramic coating has been tested for the Naval Ocean Systems Center by Hewlett-Packard Company, Solid State Laboratories, Palo Alto, CA [56]. The coating, having approximately the composition Si = 41%, O = 17% and N = 41.5% is deposited to approximately 200 Å by CVD. The fast fracture strength measures 294 KN/cm^2 for coated fibers.

We have performed coating experiments on UHV deposited samples of SiO_2 by depositing films of MgF_2, Si, Si_3N_4 or Al

on the exposed silica surface before exposure to atmospheric corrosive gases. This was viewed as auxilliary to the gaseous passivation experiments, in order to ascertain if the yield stress of UHV deposited samples could be demonstrably upgraded by physically protecting the surfaces from corrosion.

3.3.1 MgF_2 Coatings

In one experiment, MgF_2 films, 500 to 1000 Å thick, were deposited by electron beam evaporation after annealing the silica. The silica was cycled through its annealing temperature and brought down to 450°C where it remained during the second evaporation. Total elapsed time from deposition to deposition was 175 min. Auger spectra of a representative sample showed the surface composition in Table II.

The coating exhibited the proper concentration ratio of fluorine compared to magnesium in the Auger spectrometer; that is, a surface composition of 40% fluorine compared to 20% magnesium. The remainder (40%) was comprised of adsorbed carbon/oxygen gases. The fluorine to magnesium composition ratio drops as one probes deeper under the surface; but this is probably a manifestation of the differential sputtering rates of fluorine compared to magnesium.

Fracture statistics were obtained within 40 min. after extraction from the vacuum chamber (Fig. 12a) and again after samples had been incubated at 25°C at 100% relative humidity (Fig. 12b). The samples tested "dry" showed an average yield stress of 7.42 $\pm$ 0.60 KN/cm^2 and tested "wet" showed 7.64 $\pm$ .79 KN/cm^2. These results are not significantly different from the yield stresses obtained for control samples. However, the presence of MgF_2 did have a noticable effect on limiting the extent of crack propagation across the surface. When we attempted to deposit the MgF_2 before annealing the SiO_2 the test surface cracked on temperature elevation to the annealing point, presumably from thermal expansion mismatch.

3.3.2 Si Coatings

The pattern of thermal stress cracking was also observed during the rise to annealing temperature when a protective silicon coating was deposited on unannealed SiO_2. Cracking did not occur if the silica were already annealed before the amorphous Si layer was deposited. The surface of such a test sample coated with 500 Å of amorphous Si at a substrate temperature of 400°C had the composition shown in Table II.

Silicon represented 36.4% of the total elemental composition of the surface, the remaining proportions coming from adsorbed carbon (49.3%) and oxygen (14.4%) gases. The removal of material to 13 Å below the surface yielded nearly pure silicon, (94%) Si, (4%) C and (2%) O. Fracture statistics were obtained within 40 min. after exposure to ambient gases and after a 24 hr. incubation in saturated water vapor at 25°C (Fig. 13 a,b). There was not significant difference between these two groups or in comparison to the control ($\bar{\sigma}_{dry}$ = 7.83 ± 0.64 KN/cm^2 and $\bar{\sigma}_{wet}$ = 7.16 ± 0.42 KN/cm^2).

We attempted to deposit Si_3N_4 on an annealed SiO_4 film by electron beam evaporation from a powder source. This attempt was unsuccessful because the powder Si_3N_4 spattered before it evaporated, cracking the silica it contacted.

3.3.3 Metallic Coatings

Several experiments were made attempting to use Al coatings to protect the surface of deposited silica films. See ref. [57]. In one trial, 5.1μ of SiO_2 was deposited on a Mo substrate having twice the usual thickness (0.0254 cm). In another trial, 4.3μ of SiO_2 was deposited on a photoetch quality Mo substrate 0.0203 cm thick. 400 Å of Al were deposited on both test samples after completing the

annealing cycle and cooling the substrate to 200°C. The surface composition of these deposited films is shown in Table II.

Auger analysis showed the surface to be comprised of oxidized aluminum (0.65 Al:0.25 O) with some carbon contamination (0.10 C). Depth profiling showed the Al coating to be 500 Å thick, having no oxide or carbon contamination after the first few Angstroms. Fracture statistics were obtained by both three and four point bending tests (Figs. 14 a,b and 15 a,b) within 40 min. after extraction from the vacuum. Marginal improvement of the yield stress above control was noted for both samples ($\bar{\sigma}_{dry}$ = 9.8 ± .11 KN/cm^2 (3 point test) $\bar{\sigma}_{dry}$ = 9.43 ± 0.78 KN/cm^2 (4 point test) for the rectangular strips and $\bar{\sigma}_{dry}$ = 11.52 ± .43 KN/cm^2, $\bar{\sigma}_{wet}$ = 10.24 ± .26 KN/cm^2 (3 point test) for the photoetch sheets. Similar changes in the fracture stress occurred when aluminum coatings were applied to silica films which were deposited on a 0.0254 cm Mo substrate which had been hand polished to a .05μ finish (Fig. 16 a,b). That data gave mean fracture stresses of $\bar{\sigma}_{dry}$ = 11.84 ± .80 KN/cm^2 and $\bar{\sigma}_{wet}$ = 11.14 ± .73 KN/cm^2.

A summary of the mean fracture strength and standard deviation about the mean is shown in Table III for each trial coating.

3.4 Substrate and Deposited Silica Flaws

3.4.1 Substrate Roughness

The negligible to small enhancement of tensile strength over control afforded by the various surface coatings gives evidence that the fracture of deposited silica samples is not, in the main, controlled by corrosion processes, but rather by other strength controlling processes. We have looked at the matter of substrate roughness as a cause of premature fracture. The mechanism would involve the pits and rises created in both under and outer surfaces of the glass acting as stress concentrators in much the same way as cracks or notches are stress concentrators. Our attempt to reduce the likelihood of this occurrence by hand polishing Mo substrates did not raise the level of stress necessary to fracture controls. The size of flaws necessary to cause fracture at the measured tensile stresses ($\sim$ 10 KN/cm^2 may be calculated according to a formulation due to C.E. Inglis [58] (See Appendix III). The effect of large scale flaws is similar to the stress near the tip of a notch of depth c and semicircular tip radius ρ. The depth to radius ratio necessary to raise the applied stress to 80 KN/cm^2 (which is the average yield stress of a nude drawn fiber and the target value if we ignore gauge length effects) is $c/\rho \approx 12$ and that necessary to raise

the applied stress to 300 KN/cm^2 (the yeild stress of a clad fiber) is $c/\rho \gtrsim 800$. Polarizing light micrographs of surfaces of polished and unpolished Mo substrates do not show structures that would produce notches in the glass surface having depth/tip radius ratios closed to these values. Roll lines in the Mo sheet appear to have $c/\rho \gtrsim 1$. Scanning electron micrographs of unpolished Mo substrates occasionally show structure which exhibit an aspect ratio $\gtrsim 10$, but this is rare (Fig. 17a) SEM micrographs of electropolished Mo substrates on which silica films crack during annealing do not show any obvious stress concentrating structures of this description (Fig. 17b).

3.4.2 Flaws in the Silica Film

Evidence of the existence of pores in unannealed deposited silica films was presented in Fig. 4 a,b. Scanning electron micrographs did not reveal pores in annealed films, although this does not preclude their existence. We have not been able to measure any differences between the index of refraction of deposited films and that of standard fused silica plates. The index should be measurably lower in porous films [41].

3.5 Fracture Stresses for UHV Deposits having Passivation Trials by Gaseous Reagents

Although it had hitherto not been possible to show that corrosion processes were controlling the strength of the experimental deposited silica films, the possibility remained that residual vacuum chamber gases were attacking them in the lengthy interval (175 min) between the end of film deposition and the deposition of the protective coating, or that the intended protective coatings were not effective. Chamber pressure peaked to 10^{-6} torr at the highest annealing temperature and fell below 10^{-8} torr when the substrate cooled below 650°C (Fig. 9). If corrosive gases, including water vapor, were to attack the pristine silica surface before annealing while it was obviously under stress, then microcracks would have already formed on the surface prior to the deposition of a protective coating.

In order to saturate dangling bonds sticking out of the silica surface under controlled conditions, before residual chamber gases could do so, several gaseous reagents were introduced in the last minutes of SiO_2 deposition, withdrawn during annealing and readministered when the substrate temperature cooled below 650°C. Thereafter the gas was continuously leaked into the vacuum chamber at such a rate that the chamber pressure

exceeded 500 torr by the time the test sample was restored to room temperature.

3.5.1 O_2 Passivation Trials

The gases chosen to accomplish surface passivation were initially selected for their known reactivity with surface groups and from citations in the literature. Pristine silica surfaces are known to possess dangling Si bonds [59,60] which readily combine with O_2 [61] and form different binding states, up to monolayer coverage [43]. Silica films, deposited by sputtering from a vacuum melted silicon cathode in the presence of oxygen, were found to be harder than fused silica, being attacked by HF but not by H_2SO_4, HCl and HNO_3 [62,63]. These facts led to our first attempt to achieve the desired surface properties by depositing the last 5000 Å of SiO_2 in a molecular oxygen environment and by post-treating the glass in pure molecular oxygen. High purity O_2 was pre-trapped in an acetone-dry ice bath to remove contaminants like H_2O. In one experiment O_2 was leaked into the vacuum chamber to a pressure of 10^{-5} torr during the final 4 minutes of electron beam evaporation of SiO_2 and for 30 min. prior to the start of the annealing cycle. In another experiment oxygen was admitted to a pressure of 10^{-6} torr during the deposition of the last 5000 Å of SiO_2,

pumped out during the sample annealing and slowly readmitted as the sample cooled from 350°C to 25°C. The final chamber pressure was brought up to 1 atmosphere of O_2 and held overnight.

Neither of these procedures yielded samples having significantly different fracture statistics or improvement over control values. Figures (18 a,b) show the frequency distribution of fracture stresses obtained within 40 min. after extraction from the vacuum and after a 24 hr. incubation in an atmosphere at 100% relative humidity for the sample which received the shorter O_2 exposure ($\bar{\sigma}_{dry} = 7.72 \pm 1.18$ KN/cm^2 and $\bar{\sigma}_{wet} = 7.60 \pm .59$ KN/cm^2 respectively). Figures (19 a,b) show the dry and wet frequency distributions for the sample which received the longer O_2 exposure (mean values were $\bar{\sigma}_{dry} = 7.57 + .54$ KN/cm^2 and $\bar{\sigma}_{wet} = 8.20 \pm .52$, respectively).

3.5.2 Hydrogen Passivation Trials

Several studies in the literature examine the adsorption of atomic hydrogen on crystalline [64] and amorphous [65] clean Si surfaces. Both references give evidence that atomic hydrogen is capable of removing Si dangling bond surface states and provide a monolayer surface coverage. Molecular hydrogen,

on the other hand, is adsorbed only in small quantities ($\sim$ 3%) [66,67], and different binding states, perhaps associated with surface irregularities are observed [68,69]. We attempted to passivate the silica surface operating under the hypothesis that unsaturated dangling Si bonds are the sites for crack initiation. High purity molecular hydrogen was pretrapped in an acetone-dry ice bath to remove contaminants like H_2O and leaked into the system during the deposition of the last 0.1μ of silica. Exposure to atomic hydroger was made by placing the sample surface within 15 cm of the electron gun filament. The sample was exposed to 10^{-5} torr of molecular hydrogen for 10 min.; however, the exposure to atomic hydrogen was not established. After annealing, molecular hydrogen was readmitted to a pressure of 10^{-5} torr at a substrate temperature of 450°C and thereafter increased to 800 torr as the sample cooled to room temperature (25°C). It remained at 800 torr hydrogen pressure overnight.

Fracture statistics on hydrogen treated films were obtained within 40 minutes after exposure to ambient gases and after a 24 hour incubation at 100% relative humidity (Fig. 20 a,b). No significant differences were measured between these groups or and the untreated control. Mean fracture strengths measured were $\bar{\sigma}_{dry} = 8.32 \pm .99$ KN/cm^2 and $\bar{\sigma}_{wet} = 8.30 \pm .42$ KN/cm^2.

3.5.3 NH_3 Passivation Trials

Ammonia adsorbs on partially hydrophobic silica surfaces through hydrogen bonding with OH groups; the nitrogen of ammonia acting as a Lewis base for accepting the hydroxyl proton Si - OH -- $\overset{H}{\underset{H}{NH}}$ [70,21]. No evidence exists to support hydrogen bonding directly to surface oxygen atoms of the form $\begin{matrix}Si\\ \\ Si\end{matrix}\!\!>\!\!O \cdots H\,\overset{H}{\underset{H}{N}}$, but $Si - O^{-} \cdots {}^{+}H\,\overset{H}{\underset{H}{N}}$ [36] configurations are possible. The only way in which the newly deposited silica film could possess surface OH groups is presumably by the saturation of a dangling Si bond by residual water vapor within the vacuum chamber. If the newly formed surface were covered with these OH groups then they would serve as sites for the eventual nucleation of large water clusters when samples were extracted from the vacuum chamber. To prevent the nucleation of water clusters around pre-existing OH group and to saturate dangling O^{-} surface states, NH_3 gas (pretrapped in a liquid N_2 - CCl_4 slush bath) was admitted before the sample annealing at a partial pressure of 10^{-6} torr and again when the sample was cooled to 500°C. Ammonia pressure was gradually raised to 500 torr as the sample cooled to 25°C and maintained overnight. Again fracture statistics were obtained within 40 min. after sample exposure to ambient gases and after 24 hr. incubation at 100% relative humidity (Fig. 21 a,b).

Mean fracture stresses measured were $\bar{\sigma}_{dry} = 9.96 \pm 2.26$ KN/cm^2 and $\bar{\sigma}_{wet} = 8.94 \pm 1.79$ KN/cm^2. There was no significant difference between the tensile strength of these samples wet or dry and that of the control.

A summary of these gaseous passivation experiments and the resulting mean tensile strengths for UHV deposited silica films appears in Table IV.

3.6 Thermally Dehydrated Surface Treated Silica Fibers

Insofar as it became clear that fibers appear to be the best example of a flaw free, and crack free surface as is practicably attainable, they were used as model surfaces for studying the strength enhancement effects of chemisorbed gases. Though we were not equipped to clean their contaminated surfaces by ion sputtering to produce reactive, secondary surfaces; it was possible, as discussed earlier, to remove adsorbed gases by thermal pretreatment in vacuum. This process leaves the silica surface covered with silanol and siloxane groups. The surface silanol groups (SiOH) are principally of two types -- free silanols and adjacent silanols which hydrogen bond with each other. When heated under vacuum the silica surface first loses physisorbed water and then loses additional water via condensation of adjacent hydroxyls. This condensation reaction is reversible up to about 400°C.

Alcohols are known to undergo condensation reactions with the free silanol groups and the reaction is markedly enhanced by the presence of Lewis bases such as ammonia. The reaction product of N butanol ($CH_3 - CH_2 - CH_2 - CH_2OH$) and the free silanols is relatively hydrolytically stable (infra red spectra only slightly effected by exposure to 100% relative humidity at 100°C) [28]. Such an alcohol was used to prepare a (partially) hydrophobic silica surface.

The rationale for the weakening of the adsorption potential of water at a butylated silica surface follows a calculation originally performed by Babkin and Kiselev [6]. Water molecules which are adsorbed on the layer of butylsilyl groups are separated by the thickness of the modifying layer from the silicon-oxygen skeleton of the silica. Considering the hydrated (0001) face of tridymite as a model for a hydrated silica surface, Babkin and Kiselev calculated the adsorption potential for different positions above such a surface, assuming the Lennard-Jones potential. The results show that the potential due to the dispersion forces falls off rapidly with the distance from the surface, and when the adsorbed molecule is moved by the thickness of the modifying layer (7.05 Å), it acquires the character of a weak background. Furthermore, the electrostatic component of the adsorption potential is weakened owing to the dehydration of the surface.

N butanol, which was cyclically distilled under vacuum to remove soluble gases, exhibited the mass-spectrum shown in Fig. 22. This reagent was introduced as a 1:1 mixture with NH_3 into the vacuum chamber through lines which had been evacuated to 10^{-9} torr. The butanol vapors and NH_3 gas were passed through cold traps immersed in diethyleneglycol-liquid nitrogen slurries to remove any residual water vapor.

The fibers had been cut into 6 cm segments, lifted 0.0254 cm off the surface of the annealing block by two support shims placed under the opposite ends of each fiber. They were carefully supported so as not to scratch the testing surface. The fibers were dehydrated by heating up to 400°C in a vacuum of 10^{-9} torr. The gas mixture was then introduced at that temperature at a pressure of 3-5 torr. The sample was cooled slowly to room temperature thereafter.

Fracture statistics were obtained in these samples within 40 min. after extraction from the chamber using the three point bending test. The results, plotted in Fig. 23, gave a mean fracture strength of 85.87 ± 17.48 KN/cm^2, compared to 82.92 ± 23.99 KN/cm^2 for control. The fracture statistics obtained after exposure to 100% relative humidity for 24 hrs.

gave a mean fracture strength of 94.94 $\pm$ 16.12 KN/cm^2, compared to 100.46 $\pm$ 20.29 KN/cm^2 for control. Fibers which were purposefully hydrated consistently showed a higher fracture strength regardless of the imposition of an intervening hydrophobic layer. This appears to be evidence that water vapor is capable of penetrating the chemisorbed butylsilyl layer.

The lack of a demonstrable improvement in fracture strength of the treated fibers probably results from an insufficient packing density of the butylsilyl groups. One effective means of increasing the density in fibers is by pre-cleaning their surfaces to produce unsaturated Si^+ and O^- ions before passivation treatment.

4. DISCUSSION

4.1 Attempted Passivation of Silica Deposits

Two approaches were used with deposited silica samples. One involved the deposition of a surface coating of ceramic or metallic material to act as a physical barrier to the diffusion of water vapor. The other employed the chemisorption of certain gases to raise the activation energy required for the hydrolysis of surface Si-O-Si groups by water vapor.

The first approach is widely used for the protection of drawn optical fibers and was not intended as the main thrust of this research effort. It was employed to try to verify that the fracture strength of the silica deposits was controlled by a stress corrosion process. Several coating materials were used in these studies to help assure:

(a) that adequate density of surface coverage was attained and that microscopic pores in the coating were not short circuiting the water diffusion barrier.

(b) that the unsaturated surface bonds of the silica could be saturated and thereby affect a stronger cohesion between the silica and the coating.

Neither MgF_2, Si nor Al coatings improved the fracture strength of the deposits over the uncoated controls, giving strong indication that the activated reaction between water vapor and the silica front surface was not controlling the fracture strength of the test specimen. This conclusion was supported by the passivation experiments in the atomic hydrogen (H), molecular oxygen (O_2) and ammonia (NH_3) gases. H and O_2 were selected to fill the available sites on unsaturated Si^+ ions and NH_3 to saturate the oxyanions. Exposure to none of these gases increased the fracture strength of the deposits.

4.2 Errors Associated with Tensile Strength Measurements

Reference to Table III will show the fracture strength of deposits laid down on .0254 cm thick Mo sheet to be uniformly larger (by 20%) than that of deposits laid down on .0127 cm thick Mo sheet. We do not believe that this systematic difference is related to the purposeful surface treatment. There was no significant difference in yield strength determined by three and four point bending tests. The four point tests were employed to assure that no uncorrected shearing forces were causing the premature fracture of the deposits.

4.3 Comparison of Fracture Strengths of Deposits, Polished Silica Strips, and Unclad Optical Fibers

Although the UHV deposits of silica were identical to fused silica with respect to chemical composition (as judged by Auger spectra) and density (as judged by index of refraction values) the tensile strength of the deposits was about a factor of 8 less than the tensile strength of unprotected drawn fibers. Of this, perhaps a factor of 3 might be ascribed to the difference in gauge length of the samples under the testing conditions, if the same distribution of flaw sizes were present in the two cases.

The drawn glass is virtually free of microcracks when formed [71] and, unless it is inadvertently damaged mechanically in testing, exhibits a tensile strength which is apparently controlled by stress corrosion. On the other hand, the evidence is that the strength of the UHV deposits on molybdenum is controlled by flaws and internal stresses which exist even under vacuum conditions, rather than by a process involving the interaction of water vapor with the stressed glass surface.

The absence of any significant difference between the measured strengths of the polished silica strips and the UHV deposited films may have been somewhat coincidental, for it

is not necessary that the same strength controlling factors obtain in each case. The plate glass presumably is flawed by mechanical damage in the grinding operation which precedes polishing and introduces a large number of cracks that extend below the bottom of the deepest chip pits and remain after polishing. Our "diamond-scratch" tests on the plates illustrate that effect.

4.4 Causes of Premature Failure of Silica Deposits

It is entirely possible that in these films the strength controlling factors are different. Devitrification nuclei or other defects at the substrate interface, microscopic pores, and thermal microstresses are suspect causes of premature fracture in the UHV deposits.

Substrate roughness is probably not the controlling factor since, with one exception, different substrate surface roughness yielded deposits having similar fracture strengths. Electropolished substrates, which appeared to have a comparatively smooth finish, produced films which cracked on annealing. Inclusions are not considered to be a likely source of failure, since inclusions were rarely found within the deposits. They were detected early in the process of characterizing some annealed and unannealed deposits by

Scanning Electron Microscopy (SEM) and X-ray Emission Spectroscopy (KEVEX), but were not seen after changing the source cleaning procedure and after removing the tin-nickel plating on the e-gun crucible.

No conclusive evidence exists to indict a specific strength weakening mechanism, but there is an accumulation of circumstantial evidence pointing to the mentioned possibilities. The annealing of deposits at 1000°C provides an opportunity for devitrification processes to occur. Ordinarily, the crystallization requires heterogeneous nucleation, so it could begin at the under surface -- from contact with residues of a contaminated substrate, or from contact with the crystalline lattice of the substrate itself. Indeed, it has been demonstrated that moisture alone is capable of playing the role of nucleation agent [71]. The explanation for the spontaneous cracking on annealing of the deposits laid down on electropolished Mo substrates could involve the formation of devitrification nuclei by a residual contaminant coming from the electropolishing solution (875 ml CH_3OH: 125 ml H_2SO_4) which had not been removed by the usual cleaning procedures. Alternately, the etching process could have increased the microscopic surface area of the substrate or have removed part of the oxide layer which

otherwise separates film from substrate. If the devitrification nuclei had a modest under-surface density, it is feasible that the thermal stresses created during annealing could have caused the spontaneous fracture. However, such a devitrified layer of the glass would have to be very thin in order to escape detection as a translucent layer. All annealed deposits appeared to be transparent through to the substrate unless they were covered by a metallic coating.

Microscopic pores were observed by SEM only on films which were deposited at temperatures below 300°C, or which were not brought up to 1000°C for annealing. They were not detected after the sample-making procedure was changed to require deposition at 450°C and annealing at 1000°C. However, while the film porosity is clearly relieved by annealing, there is a possibility that micro-pores remain which are small enough to escape detection by SEM and which also do not measurably perturb the refractive index values.

Where the "spontaneous" fracture of unannealed glass occurred on admission of ambient atmosphere (e.g., with Ni substrates), it appears to be a clear demonstration of rapid, stress-assisted corrosion to fracture, under static (presumably tensile) stress. The fracture of samples on "high" expansion coefficient substrates on heating to the annealing temperature, are examples of fracture not caused by corrosion.

While the annealing relieves the stress originating from the film deposition, it can conceivably leave residual stresses in the composite sample due to consolidation of the SiO_2 at the annealing temperature and differential volume changes between the SiO_2 and Mo on cooling. Generally, the room temperature glass might be under compression or tension depending on the net contraction of the glass film, the deformation of the film at the annealing temperature, and the thermal contraction of the substrate. On annealing, the silica shrinks by virtue of its densification. At 1300°K, the glass at the interface with an expanded substrate is clearly under tension. As the sample is cooled to room temperature, both the substrate and film shrink, the metal mainly because of its (larger) expansion coefficient and the glass because of a free volume decrease at lower temperatures. We are not certain, therefore, of the final stress state in the glass film on the molybdenum substrate.

On the other hand, deposits on Mo left incubating in an atmosphere of saturated water vapor showed no significant impairment of strength over those tested immediately after the vacuum chamber was opened. This is in contrast to other samples (e.g. externally stressed fibers or films on higher expansion coefficient metals) which were weakened during the vapor incubation, apparently because the stress energy on exposed surfaces was sufficient to hydrolyze Si-O bonds.

This suggests that stresses at the surface of the Mo substrate samples were not a large fraction of the true fracture strength.

4.5 Water Desorption of Drawn Fibers by Heating in Vacuo

The SiO_2 deposits were intended to serve as very reactive surfaces for interaction with various gases because initially they contain many unsaturated Si^+ and O^- bonds. This not only assures the high probability for chemisorption of selected gases, it also improves the chances for dense surface coverage. Coverage by additional layers may be feasible depending on the choice of reactive groups at the non-adsorbing end of the chemisorbed gas molecules.

The use of predrawn glass fibers as model surfaces for promoting gas phase reactions has several drawbacks even if they have undergone no mechanical damage. Initially (as available, in the after-fabrication state) the surfaces are hydrated to varying degrees and the physiorbed water must be removed by heating under vacuum to about 400°C. This process leaves only two kinds of surface groups -- the siloxane Si-O-Si which is basically unreactive except when the surface is under stress; and the free silanol Si-OH

which is reactive with many gases (see Introduction). On heating the silica surface to temperatures above 500°C, many of the free surface hydroxyls which are vicinal to other hydroxyls condense to form siloxane groups and liberate water. This heating process removes many potential adsorption sites from the surface and limits the density of sites available for chemisorption. In short, the denuded fibers, as available to us, are not a satisfactory substitute for an atomically-clean surface.

The failure to show a significant increase in the fracture strength of the surface modified optical fibers by treatment with butanol and ammonia vapors indicates either that the four carbon alcohol chain is not effectively impenetrable, or that the packing density is insufficient to reduce the adsorption potential for water vapor. An effort was made to assess the surface coverage of the butyl-silyl groups by Auger spectroscopy. Unfortunately, the surface charging problem was too severe for these particular samples to obtain any reliable spectra. The fact that the surface modified fibers exhibited a slight <u>increase</u> in fracture strength after incubation in a water saturated atmosphere, as does control, indicated that water vapor was still able to penetrate the modifying layer.

5. CONCLUSIONS

This research did not accomplish the goal of demonstrating a long term enhancement of the fracture strength of SiO_2 by reducing stress corrosion through the chemisorption of passivating gases. We attempted to show, by direct mechanical testing, that chemisorbed gases could reduce the adsorption potential for water vapor to the silica surface and thereby raise the threshold stress required for the activated hydrolysis of silica bonds.

5.1 Failure of UHV Deposits to Meet Requirements that Stress Corrosion Controls Silica Strength

The major factor in the gaseous passivation approach is the requirement to produce atomically clean, and flaw free surfaces containing unsaturated Si^+ and O^- reactive centers. Samples were produced under ultrahigh vacuum conditions, treated for passivation (or coated) and then strength tested in ambient atmosphere. The major effort was concentrated on the deposition of SiO_2 as a film 3 to 5μ thick by electron beam evaporation, annealing on a molybdenum substrate and the measurement of the fracture strength of these deposits by a bend test. The results ultimately determined that the interface structure between the film and substrate was controlling the tensile strength of the film, rather than the stress corrosion of the outside surface. This finding is

not anticipated from an analysis of the tensile and shearing forces involved in the strength testing in which the sample (film on substrate) is elastically bent, with increasing curvature, over a mandrel until fracture is observed in the film. Rather, the events controlling fracture are believed to involve one or more of the following mechanisms:

(a) microscopic devitrification of the glass upon annealing, in which the substrate acts as a nucleation agent.

(b) thermal stresses left in the film from its deposition and annealing on the substrate.

(c) stress concentrating flaws either left from the deposition or replicated in the film from the substrate.

It should be pointed out that the putative thermal stresses were not experimentally measurable (the deposits on very thin Mo substrates did not curl as those on thin Ni substrates did); nor were they large enough to cause a significant change in the fracture strength of films left incubating in water saturated air for 24 hours. Neither did differences in substrate roughness, achieved by various surface treatments, cause a measurable difference in the tensile strength of the silica.

5.2 Failure of Available Drawn Fibers to Meet the Requirement that Their Surfaces be Atomically Clean

After it seemed certain that the limitations of the evaporated film technique precluded the measurement of the direct effects of surface passivation treatments on reducing stress corrosion, we resorted to cleaning the surface of existing fibers by heat treatment under UHV. Measurement of the tensile strength of unclad, untreated fibers showed them to be virtually free of surface microcracks if handled carefully. In practice, they appear to be strength limited by a stress corrosion process occurring during the strength testing. Sufficiently careful handling required that they be unclad by carbonization under electric heat, and transferred with forceps touching only the ends of test sections. Such fibers were dehydrated by heating to 400°C in ultra high vacuum, and subsequently exposed to high partial pressures of a 1:1 mixture of ammonia and N butanol. According to reference [28], N butanol undergoes surface condensation reactions with all the free hydroxyls of the silica under such conditions.

The fracture strength of these fibers was 85.87 $\pm$ 17.48 KN/cm^2 compared to 82.92 $\pm$ 23.99 KN/cm^2 control. The organic portion of the alcohol did not act as an effective barrier to prevent the corroding water vapors from reaching and reacting with the silica surface. After exposure to water saturated

air for 24 hrs., samples fractured 94.94 $\pm$ 16.12 KN/cm^2 compared to 100.46 $\pm$ 20.29 KN/cm^2 for control. The improved tensile strength of purposely hydrated fibers suggested that the beneficial effect of water vapor, in this case, might be due to rounding the surface at the tip of pre-existing cracks. The preferential etching could occur because the crack tip was presumably the only part of the fiber under a net internal stress.* These results also show that the penetration of water vapor is not significantly decreased by the interposition of a modifying layer of chemisorbed butyl groups.

There is a possibility that a longer, branching alcohol might be more effective in reducing the adsorption potential for water vapor. However, the general hydrolytic instability of a Si-O-C bond compared to a Si-O-Si bond suggests that, perhaps a more effective modification might result from the reaction of free surface hydroxyl groups with hexamethyl-disilazane.

---

* The fiber surface is thought to be under compressive stress.

The limiting factor in sample preparation by this surface cleaning approach appears to be the density with which adsorbed gases will occupy the silica surface. The surface coverage will be maximal in the case of an atomically clean, pristine surface containing unsaturated Si^+ and O^- reactive centers. Most reported studies which address the issue of gas adsorption on SiO_2 investigate the reactions on a partially dehydrated surface in which the removal of water by heating under vacuum still leaves a large part of the surface unreactive and therefore the loci for coating defects. This is, of course, the basis of our original argument for attempting passivation on a pristine, atomically clean surface.

5.3 Recommendations

The requirements that fracture test specimen be atomically clean and fracture free could be satisfied by vacuum deposited thin films of SiO_2 but were not sufficient to assure that stress corrosion was the strength controlling process. Of all the glass forms considered in this study, drawn fibers of SiO_2 appear to be the only example of a glass which is virtually fracture free initially and in which stress corrosion during the testing is the strength controlling process. Unfortunately, they are not atomically clean, as available.

Although preliminary results showed that silica surfaces easily charge and deflect a sputtering beam of argon ions enough to limit the effective depth of surface etching, it may not always be necessary to remove much surface material to produce an atomically clean and relatively crack free surface. Our work on drawn fibers indicated that their surfaces can be kept virtually crack free if they are not mechanically damaged or held under stress in a corroding atmosphere. The removal of just a few Angstroms of material is usually sufficient to produce clean surface Auger signals, and may be adequate to produce a reactive and testable sample for determining the efficacy of a particular gaseous treatment in preventing stress corrosion. Fibers appear to be the only readily available form of glass for testing the efficacy of gaseous surface passivation treatments because their fracture strength appears to be limited by the stress corrosion process. Other sample forms, which are satisfactory both from the point of view of experimental surface treatment and mechanical testing, appear to have different strength limiting structures.

Drawn fibers could be mounted in an ultra high vacuum chamber on a translation/rotation arm which moves the fiber in screw like fashion through the sputtering beam. Secondary surfaces created by this means could be exposed to various

reactive gases -- in particular, some of the substituted silanes -- and subsequently tested in ambient. To avoid the possibility that the fracture strength of these samples might also be controlled by a process other than stress corrosion, it would be important to demonstrate that they exhibit enhanced tensile strength when protected by a commonly used coating. A coating of aluminum would be easy to deposit in UHV and should render the necessary surface protection.

It should be recognized, of course, that the difficulties encountered here with developing suitable experimental samples does not indicate that it would be impossible to utilize a successful treatment in manufacture. Indeed, it seems that it will be easier to integrate a verified passivation treatment into the fiber drawing process than it has been to simulate that material with samples that satisfy both the surface chemistry requirements and the mechanical integrity needed for fracture testing.

REFERENCES

1. A. A. Griffith, Phil. Trans. Roy. Soc. London, Ser. A 221, 163 (1920).

2. J. B. Wachtman, Jr., Journ. Amer. Ceramic Soc., 57, 509 (1974).

3. S. M. Wiederhorn and L. H. Balz, Journ. Amer. Ceram. Soc., 53, 543 (1970).

4. W. B. Hillig and R. J. Charles, High Strength Materials, ed. by V. F. Zackey, John Wiley and Sons, Inc., N.Y., p. 683-705 (1965).

5. R. J. Charles, Prog. Ceram. Sci., 1, 1 (1961).

6. I. Yu. Babkin and A. V. Kiselev, Russ. Journ. Phys. Chem., 36, 1326 (1962).

7. W. A. Steele, Adv. Colloid Interface Sci., 1, 3 (1967).

8. A. R. C. Westwood and R. D. Huntington, p. 383 in Proceedings of 1971 International Conference on Mechanical Behavior of Materials, Vol. IV, The Society of Materials, Japan, 1972.

9. R. G. Greenler, J. Chem. Phys., 37, 2094 (1962).

10. O. M. Dzhigit, A. V. Kiselev and G. G. Mattik, Kolloidn, Zh., 23, 553 (1961).

11. L. D. Belyakova and A. V. Kiselev, Russ. J. Phys. Chem., 33, 39 (1959).

12. J. A. Cusumano and M. J. D. Low, Journ. of Catalysis, 23, 214 (1971).

13. B. G. Aristov and A. V. Kiselev, Russ. J. Phys. Chem., 37, 1359 (1963).

14. A. V. Kiselev, V. I. Lygin and T. I. Tal'ova, Russ. J. Phys. Chem., 38, 1487 (1964).

15. O. M. Dzhigit, A. V. Kiselev and G. G. Muttik, Kolloidn Zh., 23, 241 (1961).

16. D. Fiat, M. Folman, and U. Garbatski, J. Phys. Chem., 65, 2018 (1961).

17. O. M. Dzhigit, A. V. Kiselev and G. G. Muttik, Kolloid Zh., 24, 504 (1962).

18. G. A. Gallkin, A. V. Kiselev and V. I. Lygin, Russ. J. Phys., Chem., 36, 951 (1963).

19. L. H. Little, H. E. Klauser, and C. H. Amberg, Can. J. Chem., 39, 42 (1961).

20. L. D. Chapsman and R. McIntosh, Can. J. Chem., 40, 92 (1962).

21. M. L. Hair, Journ. Non-Crystalline Solids,19, 299 (1975).

22. D. M. Martin, Journ. Non-Crystalline Solids, 19, 285 (1975).

23. W. Hertl and M. L. Hair, J. Phys. Chem., 75, 2181 (1971).

24. K. Klier, J. H Stein and A. C. Zettlemoyer, J. Phys. Chem., 77, 1458 (1973).

25. K. R. Lange, Journ. Colloid Sci., 20, 231 (1965).

26. G. C. Pimentel and A. L. McClellan, The Hydrogen Bond, W. H. Freedman and Co., San Francisco, CA, 1960.

27. R. H. Doremus, J. Phys. Chem., 75, 3147 (1971).

28. R. G. Azrak and C. L. Angell, J. Phys. Chem., 77, 3048 (1973).

29. D. Fiat, M. Folman and U. Garbatski, Proc. Roy. Soc., A 260, 409 (1961).

30. W. Hertl, J. Phys. Chem., 72, 1248 (1968).

31. M. L. Hair and W. Hertl, J. Phys. Chem., 73, 2372 (1969).

32. W. Hertl and M. L. Hair, J. Phys. Chem., 75, 2181 (1971).

33. D. M. Martin, Journ. Non-Crystalline Solids,19, 285 (1975).

34. J. B. Peri, J. Phys. Chem.,70, 2937 (1966).

35. H. P. Boehm, M. Schneider and F. Arendt, Z. Anorg. Chem., 320, 43 (1963).

36. M. Folman, Trans. Faraday Soc., 57, 2000 (1961).

37. M. L. Hair and W. Hertl, J. Phys. Chem., 72, 16 (1973).

38. C. M. Osburn, J. Electrochem. Soc., 121, 809 (1974).

39. H. Shiraki, Jap. J. Appl. Phys., 15, 83 (1976).

40. Battelle Memorial Institute, Tech. Report AFML-TR-66-52 (1966), 5.8.2 Silicon, J. F. Lynch, C. G. Ruderer and W. H. Duckworth, eds.

41. W. A. Pliskin and P. P. Castrucci, Electrochemical Technology, 6, 85 (1968).

42. W. A. Pliskin and H. S. Lehram, J. Electrochem. Soc., 112, 1013 (1965).

43. H. Ibach and J. E. Rowe, Phys. Rev., B 9, 1951 (1974).

44. W. A. Pliskin and R. P. Esch, J. Appl. Phys., 36, 2011 (1965).

45. R. E. Mould, J. Am. Ceram. Soc., 43, 160 (1960).

46. W. Weibull, Royal Swedish Acad. of Eng. Sci. Proc., 151, 1 (1939).

47. R. Olshansky and R. D. Maurer, J. Appl. Phys., 47, 4497 (1976).

48. B. K. Tariyal and D. Kalish, Mat. Sci. and Eng., 27, 69 (1977).

49. H. Lohr, Brit. Pat, 726,312 (Nov. 1953).

50. S. Bateson and A. J. Bachmeier, Nature, London, 158, 133 (1946).

51. J. Bannon, Nature, London, 157, 446 (1946).

52. J. Bannon and C. E. Curnow, Nature, London, 161, 136 (1948).

53. M. Landau, U. S. Patent 4,188,444, Feb. 12, 1980.

54. D. G. White and E. G. Rochow, J. Am. Chem. Soc., 76, 3897 (1954).

55. T. R. AuCoin, S. DiVita, and M. J. Wade, U. S. Patent 4,118,211, Oct. 3, 1978.

56. 'High Strength Hermetically Coated Optical Fibers', Naval Ocean Systems Center, San Diego, CA 92152, Contract No. N00123-80-C-0245, by Solid State Laboratories, Hewlett-Packard Co.

57. 'The Moisture Protection of Optical Fibers', Deputy for Electronic Technology (RADC/ESM) Hanscom Air Force Base, MA, Contract No. F19628-78-C-0180 by Gulf and Western Applied Science Labs.

58. C. E. Inglis, Trans. Inst. Naval Architecture, London, 55, 219 (1913).

59. H. Hockstrasser and J. F. Antonini, Surf. Sci., 32, 644 (1972).

60. J. F. Antonini and G. Hockstrasser, Surf. Sci., 32, 665 (1972).

61. J. F. Antonini, Proc. Fourth Int. Vacuum Conf., Manchester, p. 179 (1968).

62. L. Hiesinger and H. Koenig, Festschrift 100 Jahre Heraeus Platinaschmelze, p. 376, Hanau (1951).

63. L. Holland, Vacuum Deposition of Thin Films, p. 491, John Wiley and Sons, Inc., N.Y., N.Y. (1958).

64. I. Ibach and J. E. Rowe, Surf. Sci., 43, 481 (1974).

65. J. T. Law, J. Chem. Phys., 30, 1568 (1959).

66. M. F. Chung and D. Hanemann, J. Appl. Phys., 37, 1879 (1966).

67. B. A. Joyce and J. H. Neave, Surf. Sci., 34, 401 (1973).

68. H. Ibach, K. Horn, R. Dorn and H. Lüth, Surface Sci., 38, 433 (1973).

69. B. Lang, R. W. Joyner and B. A. Somarjai, Surface Sci., 30, 454 (1972).

70. N. W. Cant and L. H. Little, Canadian Journ. Chem., 43, 1252 (1965).

71. F. M. Ernsberger, Proc. First Tewksbury Symposium, Univ. of Melbourne, Univ. of Melbourne Press, p. 104 (1963).

72. H. D. Conway, Phil. Mag., 38, 905 (1947).

73. R. D. Schele and R. L. Sierakowski, J. Non-Linear Mechanics 2, 61 (1967).

74. E. Orowan, Classical and Dislocation Theories of Brittle Fracture, p. 147-160, In Conf. on Fracture; Fracture Proceedings (1959).

TABLE I

Thickness, Refractive Index and Composition
of Some Untreated, Deposited Films

Substrate	Deposit Thickness Microns	Refractive Index (6328A)	Composition Si	Composition O	Preparation Conditions
Ni	4.8	1.42	0.32	0.68	deposited @ 280°C; unannealed film cracked and peeled off substate on exposure to ambient gases
Ni	2.93	1.44	0.35	0.65	deposited @ 280°C; annealed @ 980°C for 20 min., film cracked in chamber during annealing
Mo	0.2	1.46	0.33	0.67	deposited @ 450°C; annealed @ 980°C for 20 min., film completely intact.
Mo	2.55	1.44	0.31	0.69	deposited @ 450°C, unannealed film completely intact.
Pd	5.33	--	--	--	deposited @ 450°C; annealed at 1000°C for 1 hr., film cracked in chamber during annealing
Ta	5.12	--	--	--	deposited @ 450°C, annealed at 1000°C for 1 hr., film cracked in chamber during annealing

TABLE II

The Thickness and Composition of Some Surface Treated, Deposited Films

Deposit Thickness (microns)	Index Refraction n (6328 Å)	Depth below Surface (Å)	Composition						Surface Treatment
			Si	O	C	Mg	F	Aℓ	
1.0	1.46	---	---	---	---	---	---	---	exposure to 2×10^{-2} torr-sec. O_2 prior to annealing
3.46	1.46	0	0.24	0.55	0.21	---	---	---	exposure to 6×10^{-5} torr-sec. O_2 prior to annealing and to 760 torr O_2 for 12 hrs. after annealing
		200	0.31	0.68	0	---	---	---	
2.05	1.46	0	0.27	0.59	0.14	---	---	---	exposure to 3×10^{-3} torr sec. H_2 under conditions which will dissociate H_2 and 1000 torr H_2 for 12 hrs. after annealing
		200	0.33	0.67	0	---	---	---	
3.5	1.46	0	0.24	0.62	0.14	---	---	---	exposure to 1.8×10^{-3} torr-sec. NH_3 immediately following annealing and slowly brought up to 500 torr NH_3 as sample cooled. Left at 500 torr NH_3 for 12 hrs.
3.6	---	0	0	.33	.07	.21	.39	---	sample annealed under 10^{-6} torr, then MgF_2 deposited at substrate temperature of 450°C
		200	.12	.18	.16	.40	.15	---	
		700	.33	.67	0	0	0	---	
3.7	---	0	0.36	0.14	0.5	---	---	---	sample annealed under 10^{-6} torr then Si deposited at substrate temperature of 400°C
		13	0.94	0.02	0.04	---	---	---	
		400	0.44	0.67	0	---	---	---	
4.3	---	0	0	0.25	0.01	---	---	0.65	sample annealed under 10^{-6} torr then Aℓ deposited at substrate temperature of 200°C
		600	0.67	0.33	0	---	---	0	

* Crater depths are based upon sputtering times and a sputtering rate of 133 Å/min. for SiO_2.

TABLE III

Tensile Strength of SiO_2 Deposits Receiving Hermetic Protection by Various Coatings

Hermetic Coating	SiO_2 Thickness (microns)	Substrate Thickness (cm)	Mean Tensile Strength tested dry (KN/cm^2)	Mean Tensile Strength tested wet (KN/cm^2)
Control	0.2	.0127	8.46 ± 1.92 (3 pt)	7.80 ± .58
	3.88	.0127	7.65 ± 1.51 (4 pt)	-----
MgF_2	3.6	.0127	7.42 ± 0.60 (3 pt)	7.64 ± .79
Si	5.25	.0127	7.83 ± .64 (3 pt)	7.16 ± .42
Al	5.1	.0254	9.81 ± .11 (3 pt)	-----
			9.43 ± .78 (4 pt)	-----
"	4.8	.0254	11.84 ± .80 (3 pt)	11.14 ± .73
"	4.3	.0203	11.52 ± .43 (3 pt)	10.25 ± .26

TABLE IV

Tensile Strength of SiO_2 Deposits Receiving Surface Modification by Adsorption of Various Gases

Pre-annealing Gas Exposure	SiO_2 Thickness	Substrate Thickness (cm)	Mean Tensile Strength tested dry (KN/cm^2)	Mean Tensile Strength tested wet (KN/cm^2)
Control	0.2 μ	0.0127	8.46 ± 1.92 (3 pt)	7.80 ± .58
	3.88μ	0.0127	7.65 ± 1.51 (4 pt)	-----
2×10^{-2} torr-sec O_2	1.0 μ	0.0127	7.72 ± 1.18 (3 pt)	7.60 ± .59
6×10^{-4} torr-sec O_2	3.46μ	0.0127	7.57 ± .54 (3 pt)	8.20 ± .52
3×10^{-3} torr-sec H_2	2.05	0.0127	8.32 ± .99 (3 pt)	8.30 ± .42
1.8×10^{-3} torr sec NH_3	3.49	0.0127	9.96 ± 2.26 (3 pt)	8.94 ± 1.79

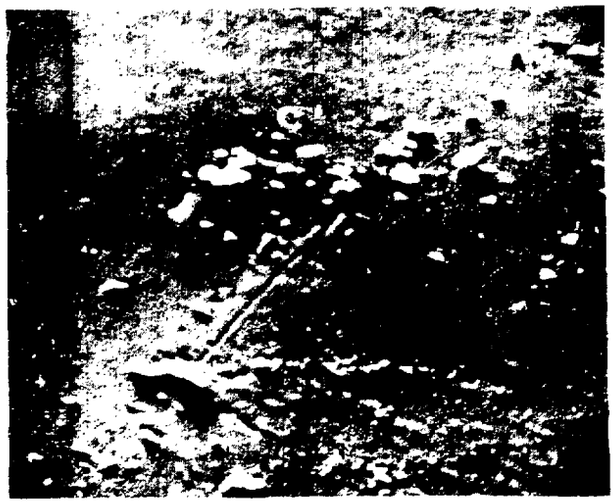

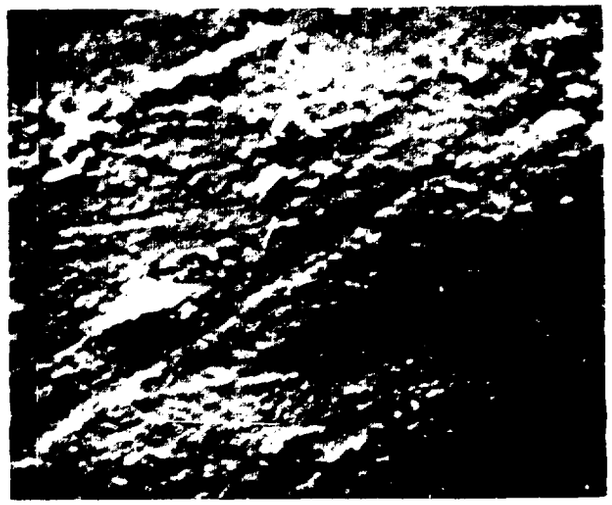

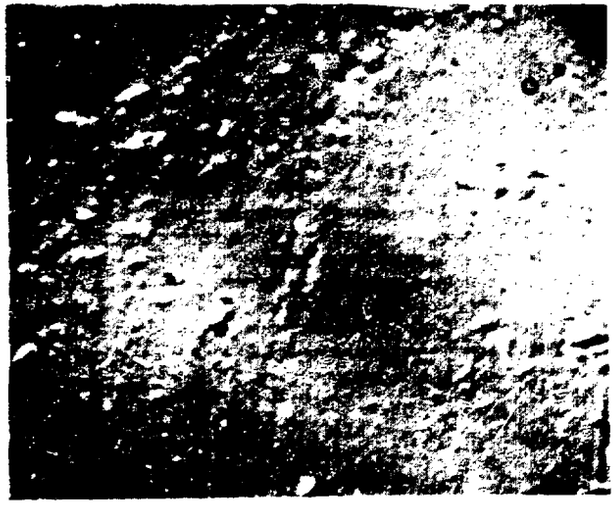

FIGURE 1

SEM photographs of the mirror zone of a fracture surface of fused silica (Amersil Suprasil II). This surface was abraded as described in the text (Sec. 2). Fig. 1, a and b show the surface before argon ion bombardment. Fig. 1, c shows the same surface following 1.5 hr. exposure to a 4 KV beam of Ar^+. (Magnification: Fig. 1 a,b 4068X, 1 mm = 0.25μ, Fig. 1c 4350 x 1 mm = 0.23μ.)

FIGURE 2

Facility for depositing silica films in ultra high vacuum.

a. film deposition quartz monitor sensor head

b. molybdenum annealing block

c. evaporation shutter

d. charge of SiO_2 in crucible of three crucible e-gun evaporator

e. molybdenum radiation shield (top shield was removed for picture clarity).

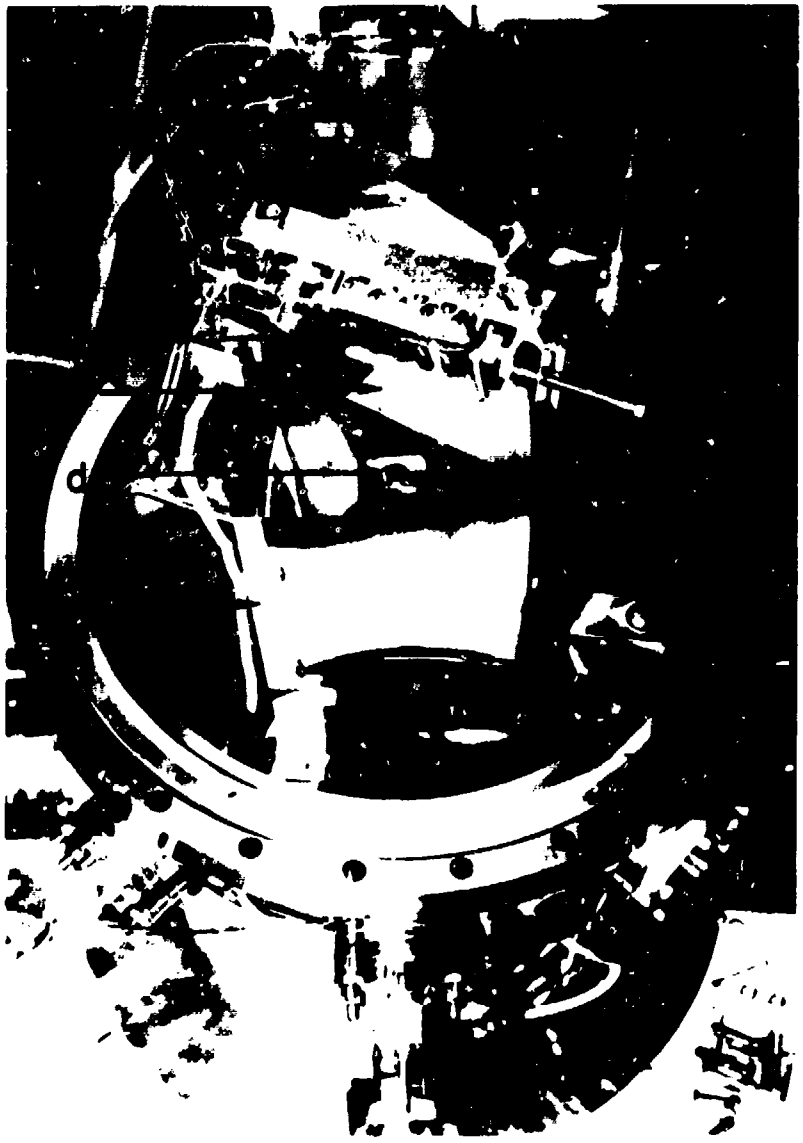
d

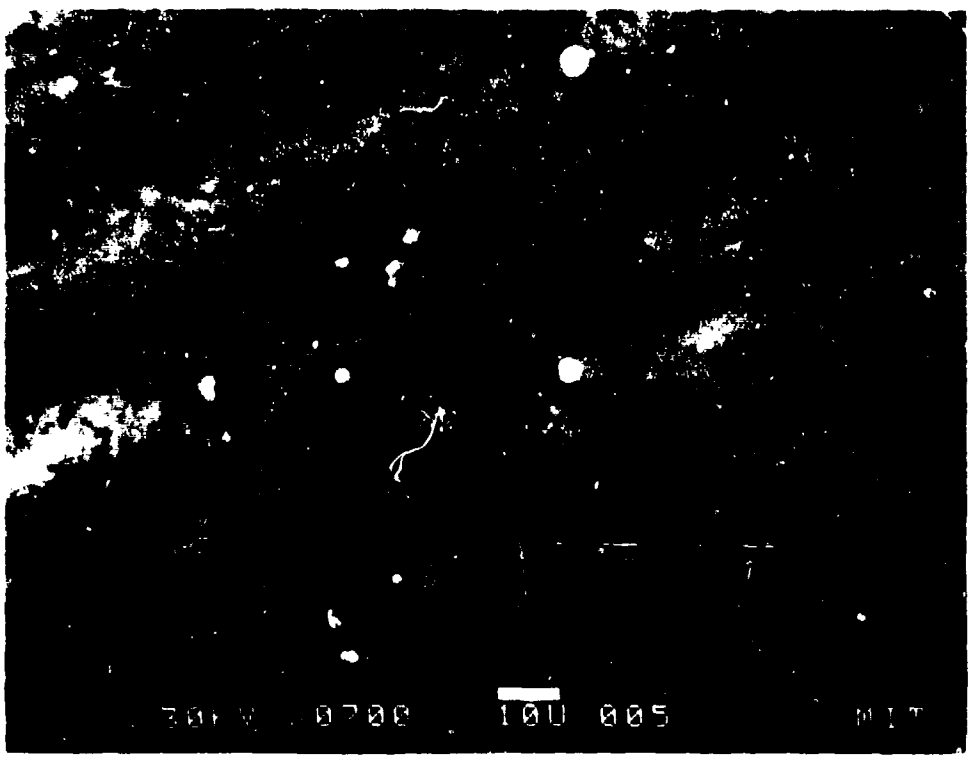

FIGURE 3

SEM photograph of the surface of an unannealed silica film deposited on a Ni substrate, showing microscopic pores (some about 1μ across) associated with a lack of densification.

FIGURE 4

SEM photographs of the surfaces of unannealed (4a,4b) and annealed (4c,4d) silica films deposited on Mo substrates. Conditions of evaporation were as described in the text. Figures 4a, 4b show microscopic pores in addition to the general surface roughness. Figures 4c, 4d show a portion of the annealed silica surface after strength testing, in which a square chip of film was thrown up from the surface, providing a view of a cross section through the film. Roll marks arising from substrate manufacture are visible as contours on the film.

A

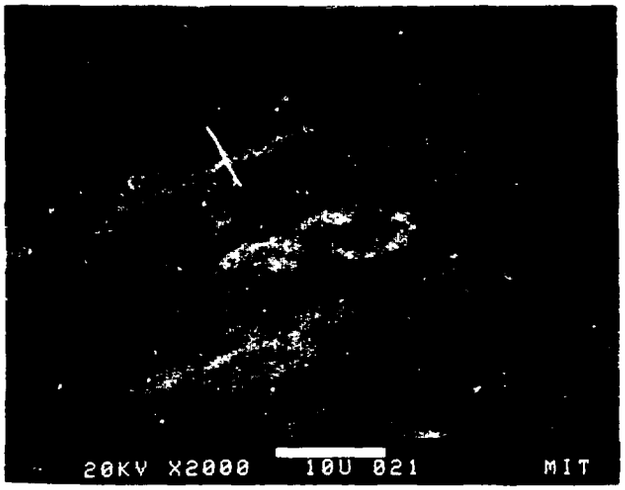
20KV X2000 10U 021 MIT

B

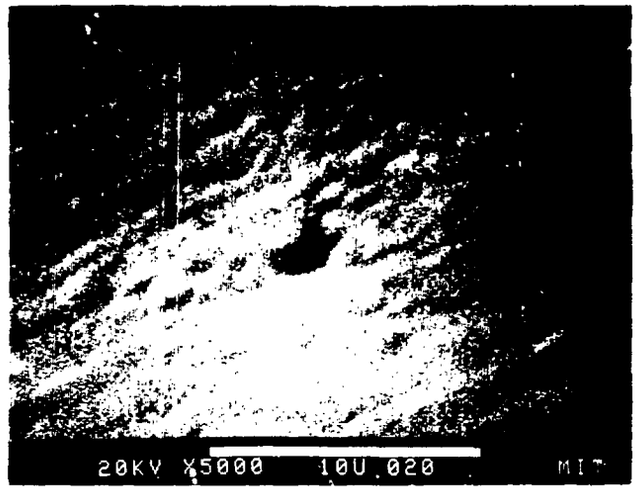
20KV X5000 10U 020 MIT


20KV X200 100U 016 MIT


20KV X4000 10U 015 MIT

FIGURE 5

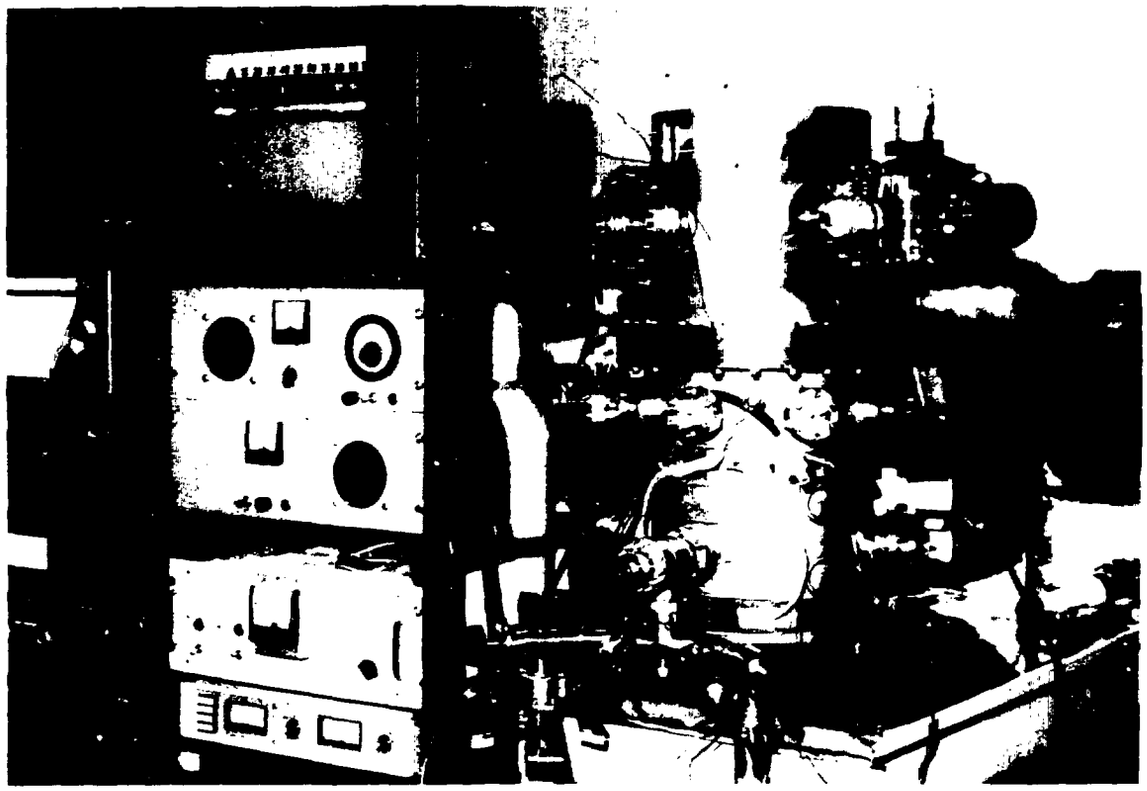

UHV chamber for depositing silica films, Instrumentation panels include (clockwise from left): power supply for e-gun evaporator, strip chart recorders, titanium sublimation pump control, substrate block temperature control, ion pump control, and ionization gauge control.

FIGURE 6

a. Bending jig for measuring tensile strength under three and four point loads.

b. Close up view of center and outer film supports. Vernier scale measures 10X the actual angle of rotation of the pins which support the film at its ends. The central support shown in b is a 10° included angle knife edge. (Not shown is the alternate central support for four point bending.) The outer pins rotate about the axis which is coincident with the tip of the central knife edge. The radius of rotation is 0.7925 cm.

A

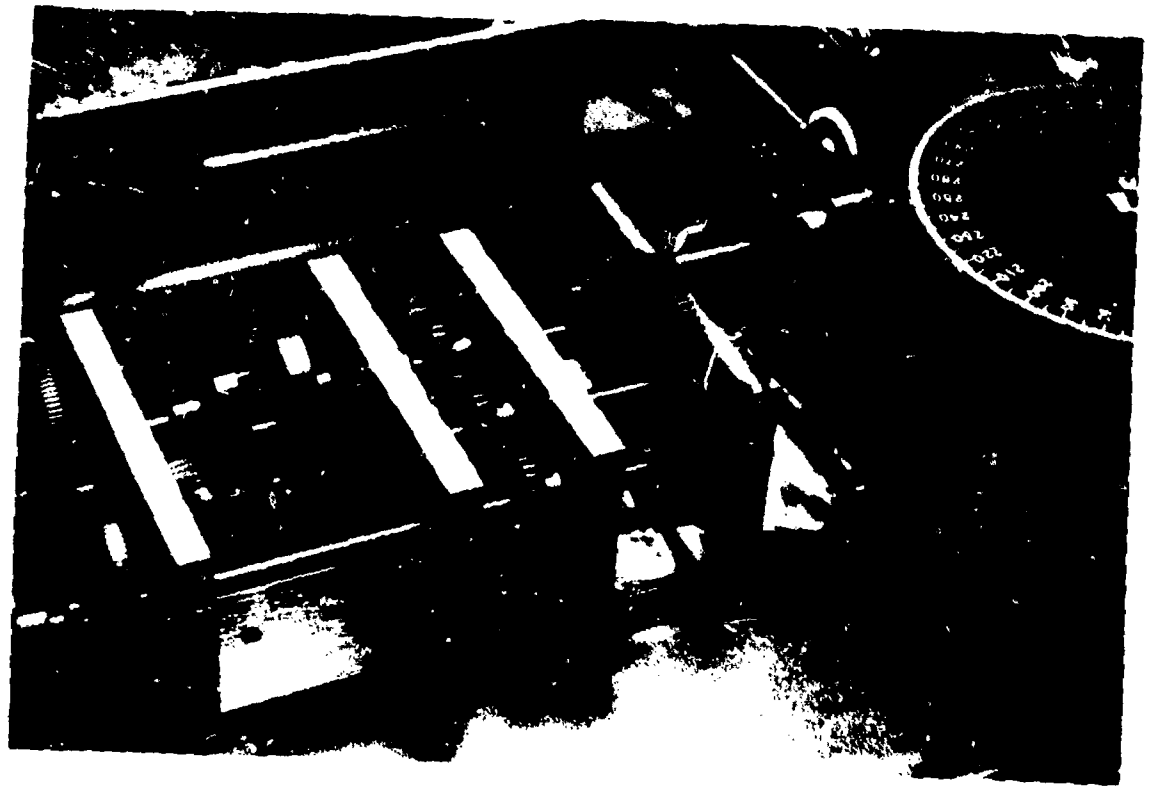

B

FIGURE 7

The frequency distribution of fracture strengths measured for a 200μ diameter optical fiber guide. The frequency distribution is expressed as a percentage of total sample size (N) and tensile stress is expressed in KN/cm^2. All fibers were tested, after plastic cladding had been removed by carbonization under electric heat, by the three point bend test.

a. The frequency distribution versus tensile strength for fibers tested within 40 min. after the removal of the plastic coating. mean tensile strength: 82.92 ± 23.99 KN/cm^2.

b. The frequency distribution versus tensile strength for fibers tested after cladding material was removed and after a 24 hr. incubation in air saturated with vapor. mean tensile strength: 100.46 ± 20.29 KN/cm^2.

c. The frequency distribution versus tensile strength for declad fibers which had been wrapped around a 9.9 cm diameter mandrel and kept in a water saturated atmosphere for 24 hrs. prior to testing. mean tensile strength: 68.28 ± 17.49 KN/cm^2.

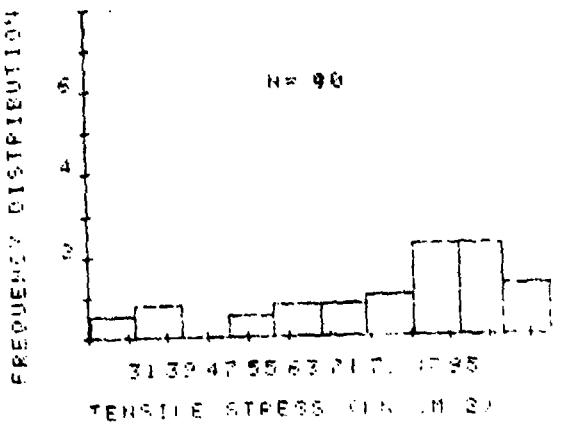
N= 90
FREQUENCY DISTRIBUTION
TENSILE STRESS (KN CM 2)

A

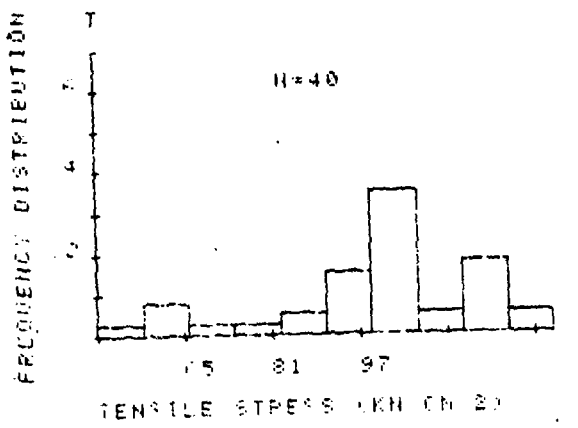
N=40
FREQUENCY DISTRIBUTION
TENSILE STRESS (KN CM 2)

B

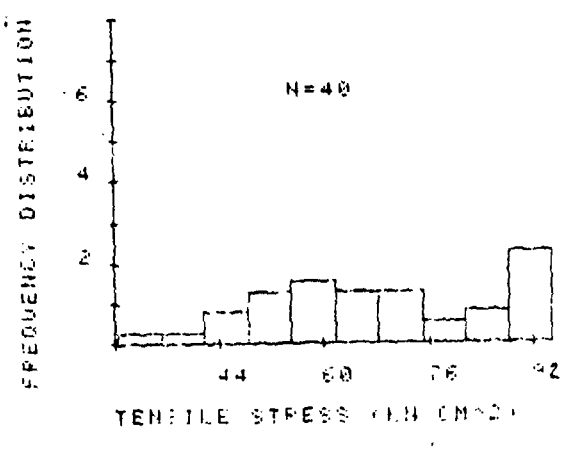
N=40
FREQUENCY DISTRIBUTION
TENSILE STRESS (KN CM-2)

C

FIGURE 8

The frequency distribution of fracture strengths measured for polished silica strips having the same dimensions as the UHV deposits. The dimensions are as given in the text. The frequency distribution is expressed as a percentage of the total sample size (N) and tensile stress is expressed in KN/cm^2.

a. Mean tensile strength: 12.37 ± 1.76 KN/cm^2.

b. Fracture statistics obtained after abrading the surface by lightly scratching with a diamond tip stylus.
Mean tensile strength: 5.90 ± 1.13 KN/cm^2.

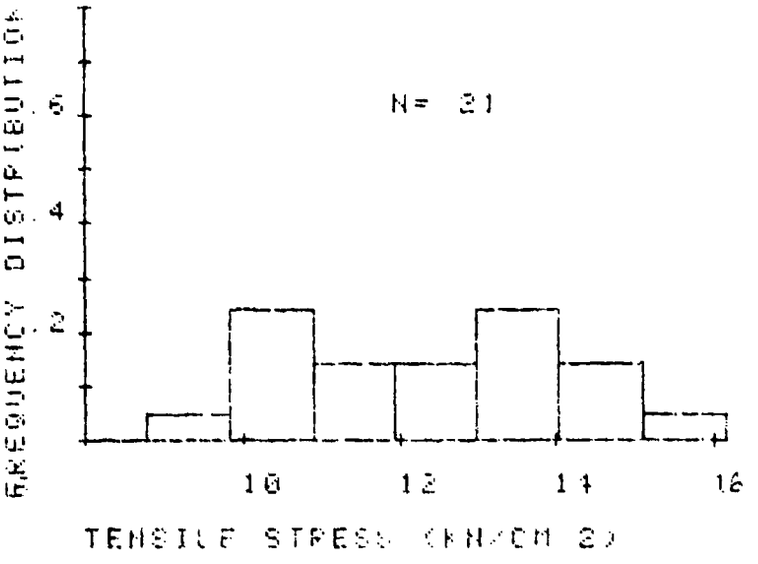
FREQUENCY DISTRIBUTION
N= 31
2
4
6
10
12
14
16
TENSILE STRESS (KN/CM 2)

A

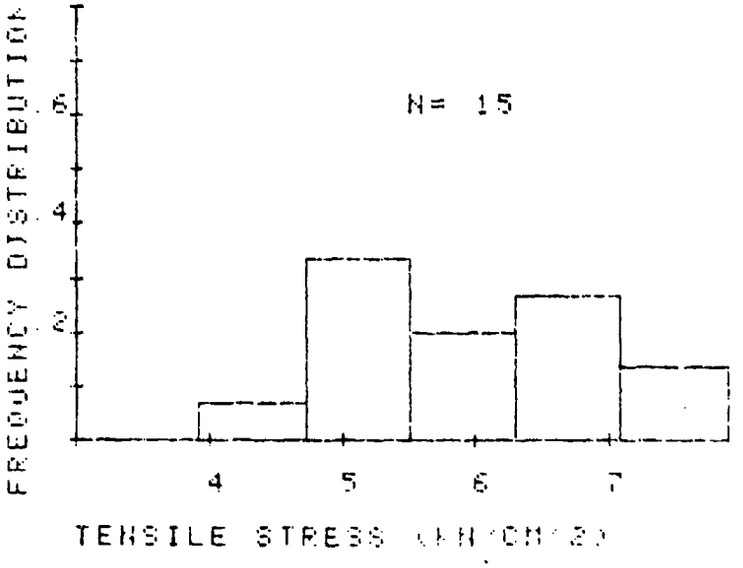
FREQUENCY DISTRIBUTION
N= 15
2
4
6
4
5
6
7
TENSILE STRESS (KN/CM 2)

B

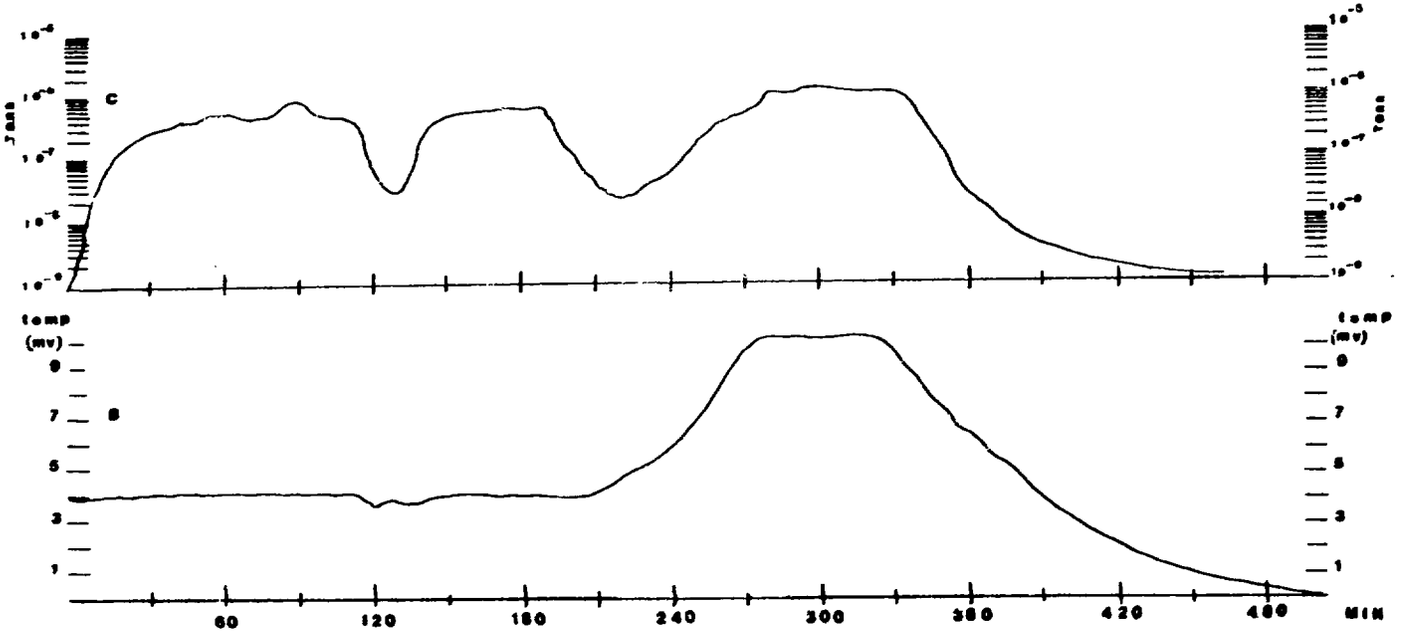

FIGURE 9

The time course of a representative sample preparation in UHV, showing

(a) the film deposition rate

(b) the sample temperature variations

(c) the chamber pressure variations

The measurement of these parameters is described in the text.

FIGURE 10

The frequency distribution of fracture strengths for UHV deposited films which received no surface treatment. The frequency distribution is expressed as a percentage of the total sample size (N) and the tensile stress is expressed in KN/cm^2. SiO_2 deposits are 3.9μ thick.

a. the results of the three point bend tests for control deposits tested after exposure to ambient gases for up to 40 min. mean tensile strength: 8.46 ± 1.92 KN/cm^2.

b. the results of the four point bend tests for control deposits tested after exposure to ambient gases for up to 40 min. mean tensile strength: 7.65 ± 1.51 KN/cm^2.

c. the results of the three point bend tests for control deposits tested after exposure to 100% relative humidity for 24 hrs. mean tensile strength: 7.80 ± 0.58 KN/cm^2.

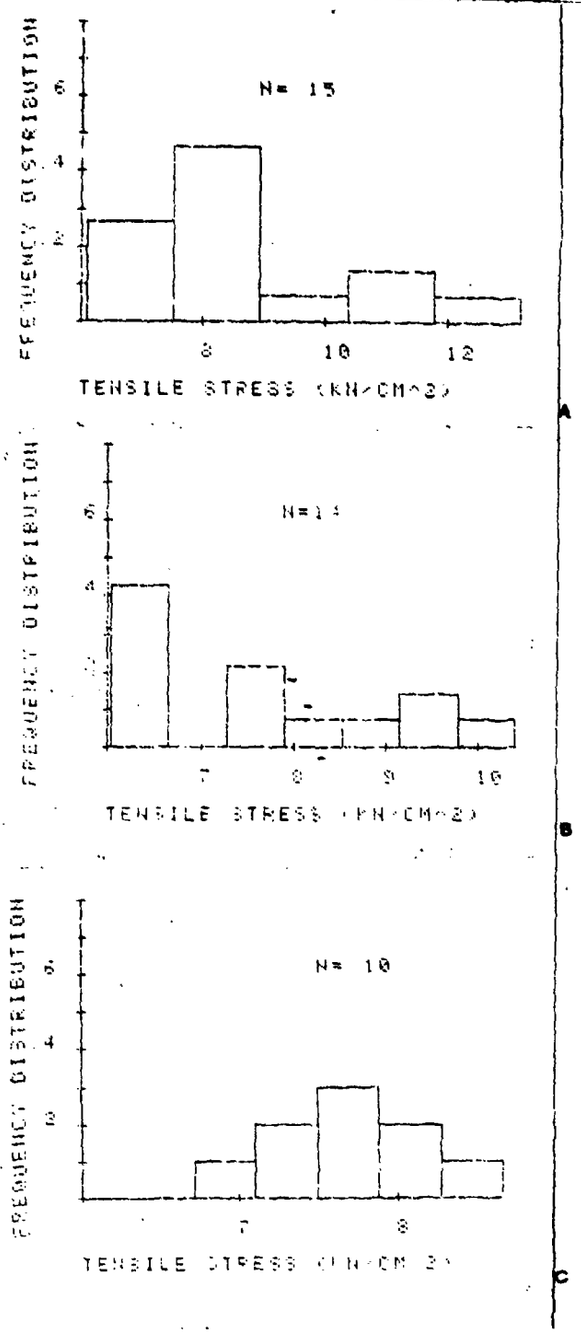
FREQUENCY DISTRIBUTION
N= 15
8
10
12
TENSILE STRESS (KN/CM^2)
A
FREQUENCY DISTRIBUTION
N=14
7
8
9
10
TENSILE STRESS (KN/CM^2)
B
FREQUENCY DISTRIBUTION
N= 10
7
8
TENSILE STRESS (KN/CM^2)
C

FIGURE 11

Polarizing light micrographs showing the surface morphology of molybdenum substrates which had received different surface treatments. Magnification 30X.

a. Standard quality, rolled Mo sheet (Alpha Division, Ventron Corporation) (depth of pits estimated to be 2 microns).

b. Photoetch quality Mo sheet (Metallwerk Plansee, Schwarzkopf Development Corporation) having roll marks mostly one directional. (depth of pits estimated to be 2 microns).

c. Electropolished standard quality, rolled Mo sheet (depth of pits estimated to be 2 microns).

d. Hand polished standard quality rolled Mo sheet (depth of largest pits estimated to be 3 microns).

(Depths estimated by depth of field adjustment on microscope).

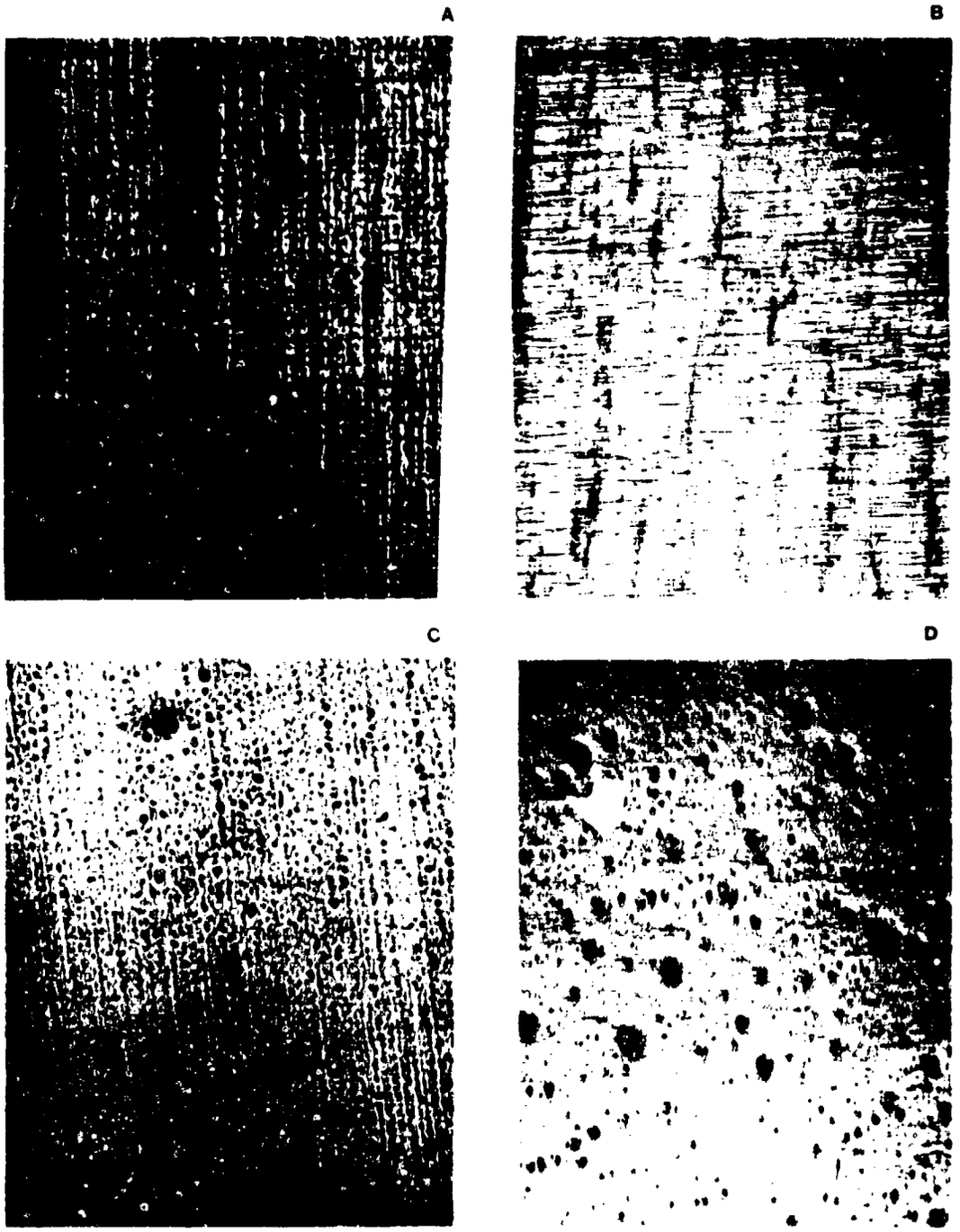
A
B
C
D

FIGURE 12

The frequency distribution of fracture strengths for UHV deposits receiving a 700 Å coating of MgF_2. Frequency distribution is expressed as a fraction of the total sample size (N) and tensile stress is expressed in KN/cm^2, SiO_2 deposits are 3.6μ thick.

a. The fracture statistics obtained with a three point bend test on a 0.0127 cm thick standard substrate. Exposed to ambient gases for up to 40 min. prior to testing. Mean fracture strength: $7.42 \pm .60$ KN/cm^2.

b. Same preparation exposed to 100% relative humidity for 24 hrs. prior to testing mean fracture strength: $7.64 \pm .79$ KN/cm^2.

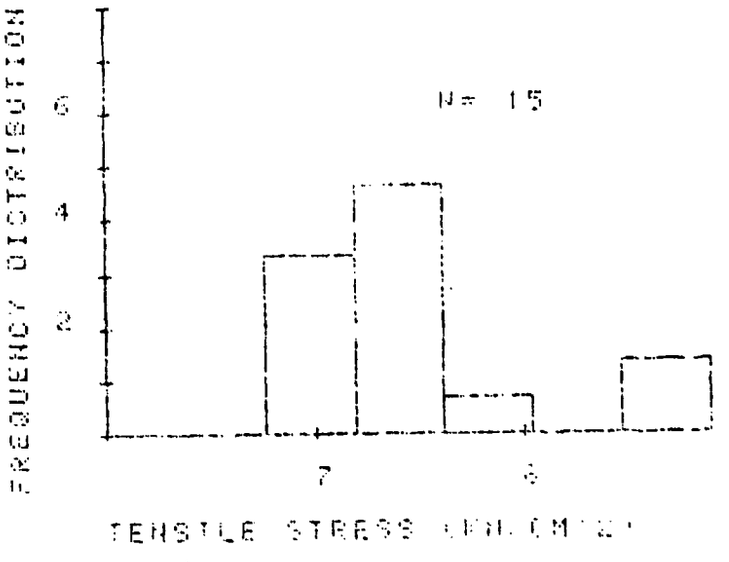
FREQUENCY DISTRIBUTION
N= 15
2
4
6
7
8
TENSILE STRESS (KN./CM**2)

A.

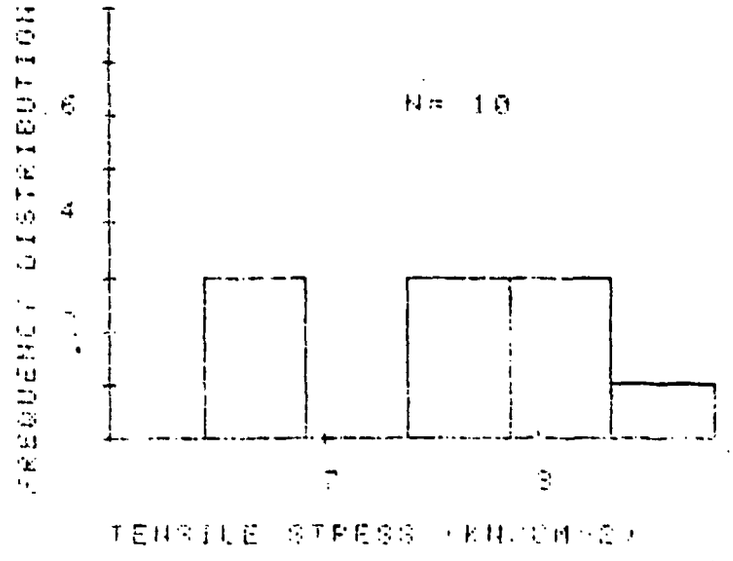
FREQUENCY DISTRIBUTION
N= 10
4
6
7
8
TENSILE STRESS (KN./CM**2)

B

FIGURE 13

The frequency distribution of fracture strengths for UHV deposits receiving a 400 Å coating of Si. SiO_2 Deposits are 5.3μ thick.

a. The fracture statistics obtained with a three point bend test on a 0.0127 cm thick standard substrate. Exposed to ambient gases for up to 40 min. prior to testing. Mean fracture strength: 7.83 $\pm$ .64 KN/cm^2.

b. Same sample preparation exposed to 100% relative humidity for 24 hrs. prior to testing.
Mean fracture strength: 7.16 $\pm$ .42 KN/cm^2.

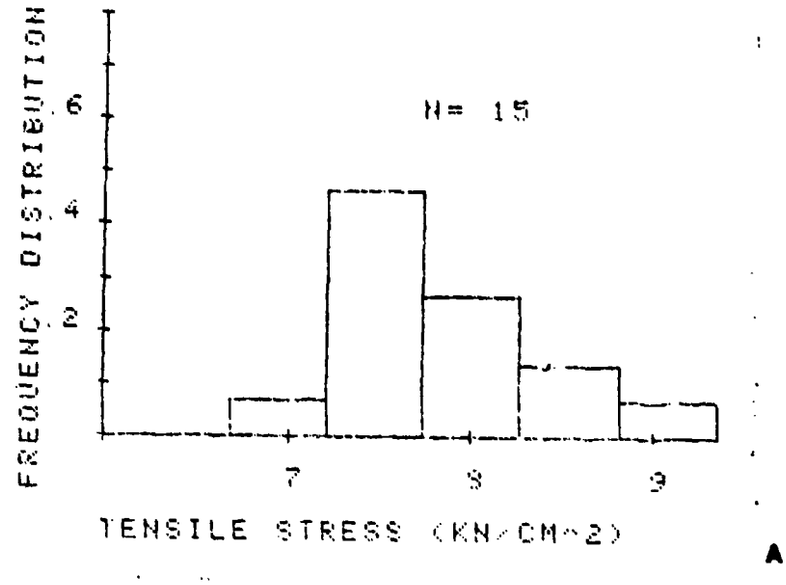
FREQUENCY DISTRIBUTION
N= 15
TENSILE STRESS (KN/CM^2)

A

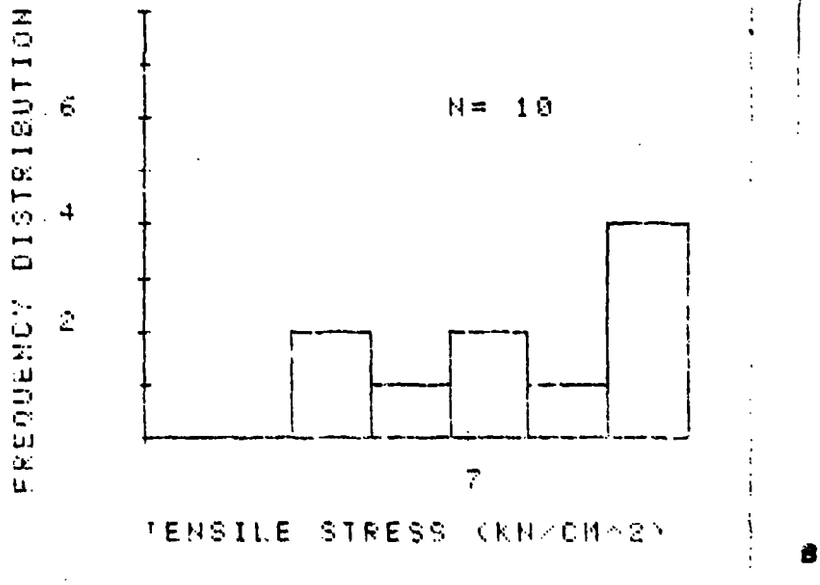
FREQUENCY DISTRIBUTION
N= 10
TENSILE STRESS (KN/CM^2)

B

FIGURE 14

The frequency distribution of fracture strengths for UHV deposits receiving a 400 Å coating of Aℓ. SiO_2 deposits are 5.13μ thick.

a. The fracture statistics obtained with a three point bend test on a 0.0254 cm thick standard substrate. Exposed to ambient gases for up to 40 min. prior to testing. Mean fracture strength: 9.81 $\pm$ .11 KN/cm^2.

b. The fracture statistics obtained on the same sample with a four point bend test. Mean fracture strength: 9.43 $\pm$ .78 KN/cm^2.

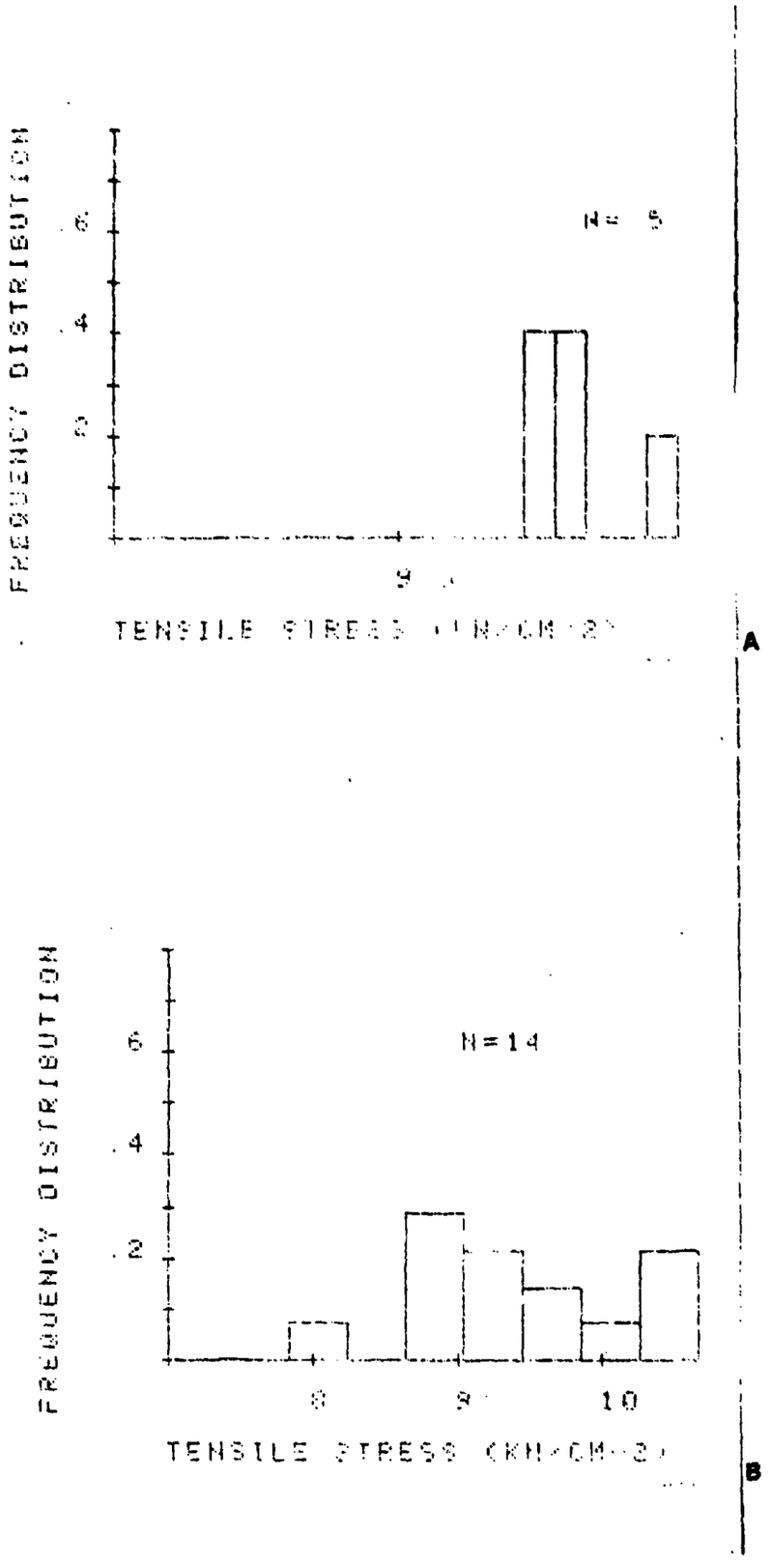
FREQUENCY DISTRIBUTION
N = 5
TENSILE STRESS (KN/CM-2)
A
FREQUENCY DISTRIBUTION
N=14
8
10
TENSILE STRESS (KN/CM-2)
B

FIGURE 15

The frequency distribution of fracture strengths for UHV deposits receiving a 400 Å coating of Aℓ. SiO_2 deposits are 4.3μ thick.

a. The fracture statistics obtained with a three point bend test on a 0.0203 cm thick photoetch quality substrate. Exposed to ambient gases for up to 40 min. prior to testing.
mean fracture strength: 11.52 $\pm$ .43 KN/cm^2.

b. Same sample preparation exposed to 100% relative humidity for 24 hrs. prior to testing.
mean fracture strength: 10.25 $\pm$ .26 KN/cm^2.

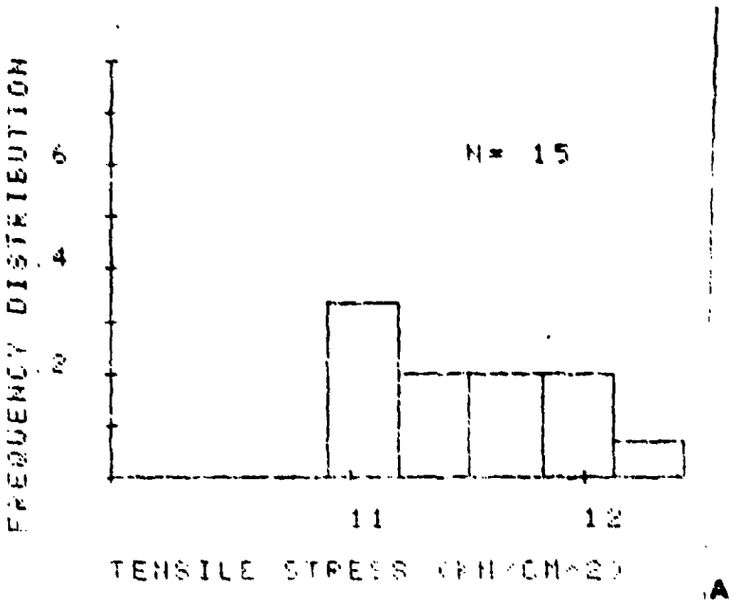
FREQUENCY DISTRIBUTION
N= 15
11
12
TENSILE STRESS (KN/CM^2)

A

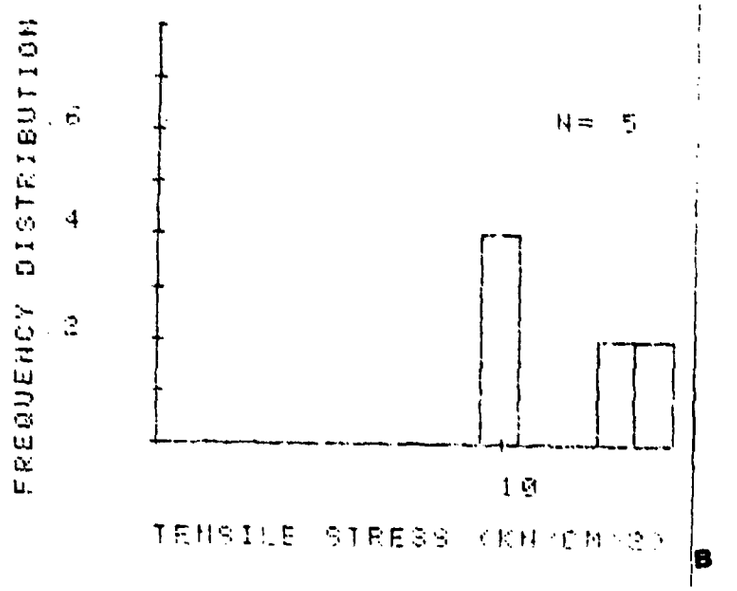
FREQUENCY DISTRIBUTION
N= 5
10
TENSILE STRESS (KN/CM^2)

B

FIGURE 16

The frequency distribution of fracture strengths for UHV deposits receiving a 500 Å coating of Aℓ. SiO_2 deposits are 4.8μ thick.

a. The fracture statistics were obtained with a three point bend test on a 0.0254 cm thick, hand polished substrate and exposed to ambient gases for up to 40 min. prior to testing.
Mean fracture strength: 11.84 $\pm$ .80 KN/cm^2.

b. Same sample preparation exposed to 100% relative humidity for 24 hrs. prior to testing.
Mean fracture strength: 11.14 $\pm$ .73 KN/cm^2.

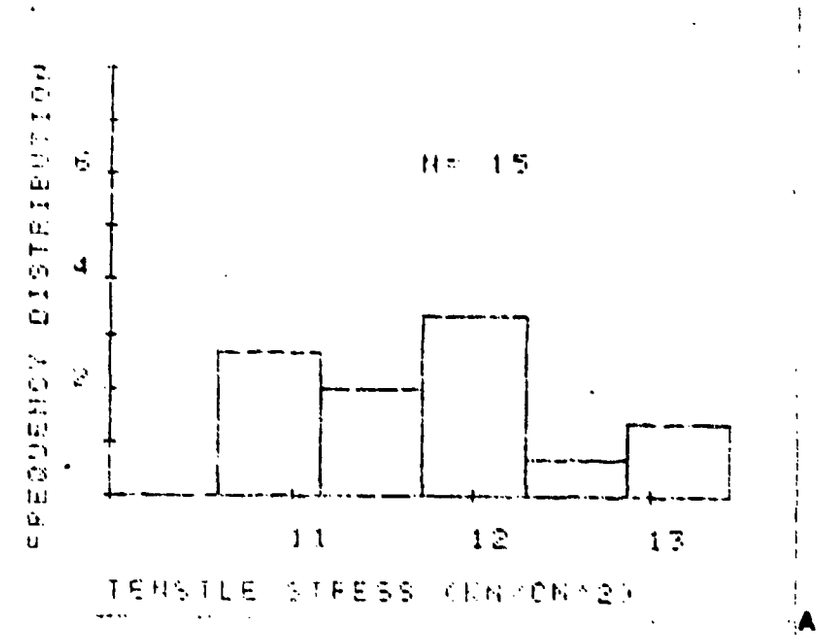
FREQUENCY DISTRIBUTION
N= 15
4
2
11
12
13
TENSILE STRESS (KN/CM^2)

A

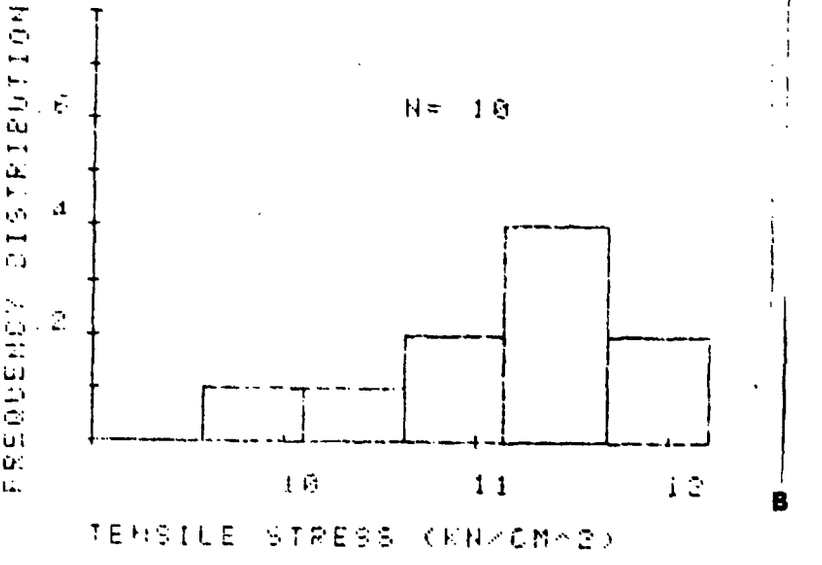
FREQUENCY DISTRIBUTION
N= 10
4
2
10
11
12
TENSILE STRESS (KN/CM^2)

B

FIGURE 17

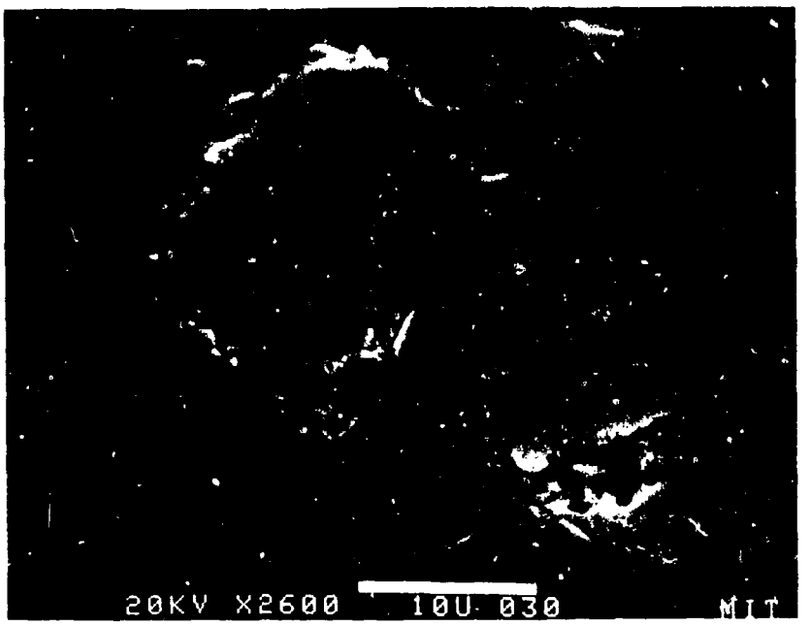

SEM photographs of a flaw in a standard 0.0127 cm thick Mo sheet (a) and a similar sheet after electropolishing (b).

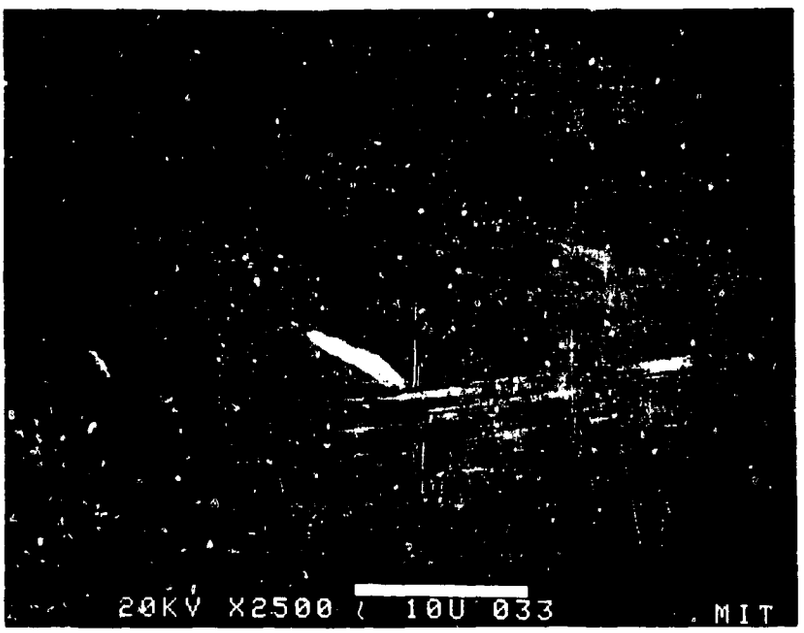

FIGURE 18

The frequency distribution of fracture strengths for UHV deposits receiving 2×10^{-2} torr-sec. exposure to O_2 before annealing. SiO_2 deposits are 1.0μ thick.

a. The fracture statistics were obtained with a three point bend test on a 0.0127 cm thick substrate. Samples were exposed to ambient gases for up to 40 min. prior to testing.
Mean fracture strength: 7.72 ± 1.18 KN/cm^2.

b. Same sample preparation exposed to 100% relative humidity for 24 hrs. prior to testing.
Mean fracture strength: $7.60 \pm .59$ KN/cm^2.

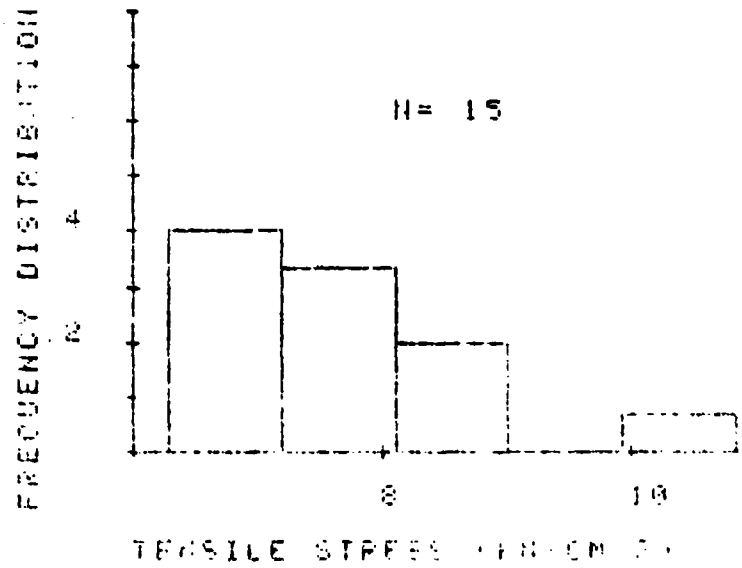

TENSILE STRESS (KN/CM 2)

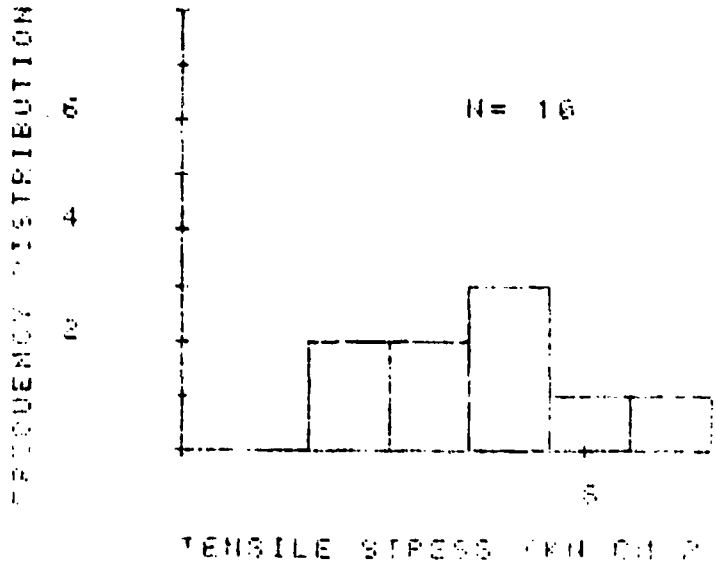

TENSILE STRESS (KN/CM 2)

A

B

FIGURE 19

The frequency distribution of fracture strengths for UHV deposits receiving 6×10^{-4} torr-sec. exposre to O_2 before annealing and 760 torr O_2 for 12 hrs. after annealing. SiO_2 deposits are 3.46μ thick.

a. The fracture statistics were obtained as in Fig. 18a.
Mean fracture strength: $7.57 \pm .54$ KN/cm^2.

b. The fracture statistics were obtained as in Fig. 18b.
Mean fracture strength: $8.20 \pm .52$ KN/cm^2.

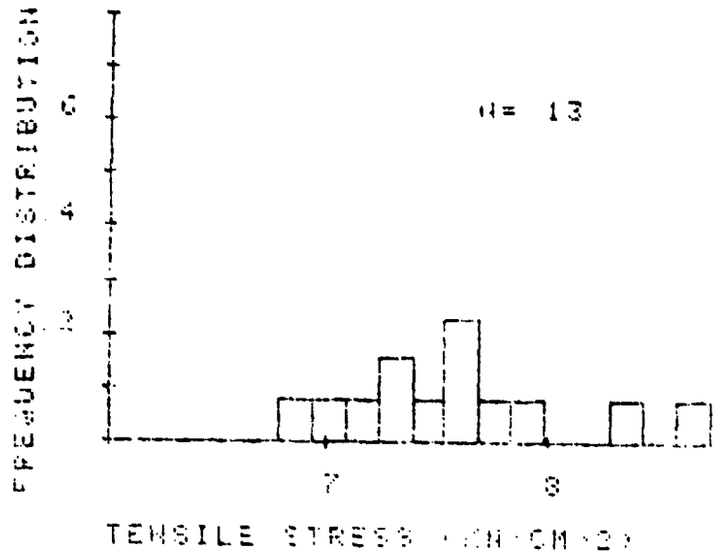
FREQUENCY DISTRIBUTION
N= 13
4
2
7
8
TENSILE STRESS (KN·CM·2)

A

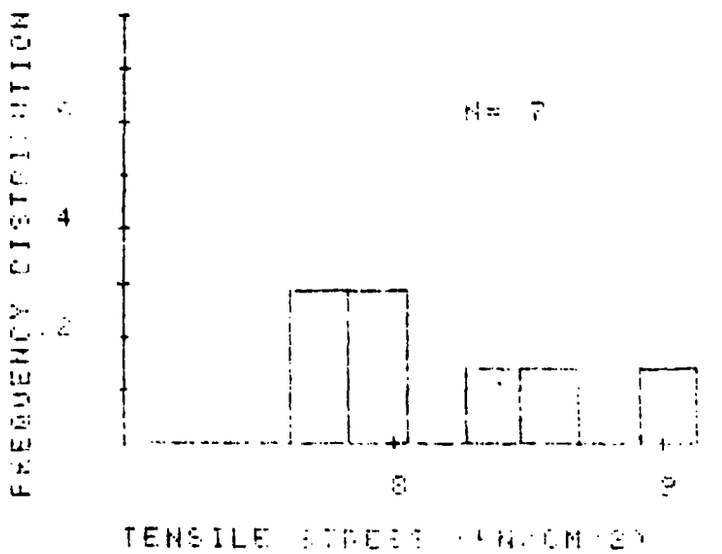
FREQUENCY DISTRIBUTION
N= 7
4
2
8
9
TENSILE STRESS (KN·CM·2)

B

FIGURE 20

The frequency distribution of fracture strengths for UHV deposits receiving 3×10^{-3} torr-sec. exposure to H_2 before annealing and 1000 torr H_2 for 12 hrs. after annealing.
SiO_2 deposits are 2μ thick.

a. The fracture statistics were obtained as in Fig. 18a.
Mean fracture strength: $8.32 \pm .99$ KN/cm^2.

b. The fracture statistics were obtained as in Fig. 18b.
Mean fracture strength: $8.30 \pm .42$ KN/cm^2

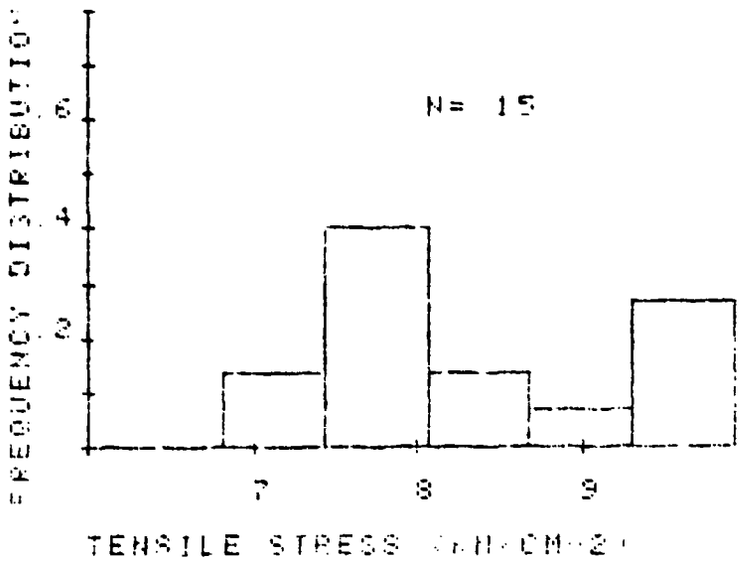

A

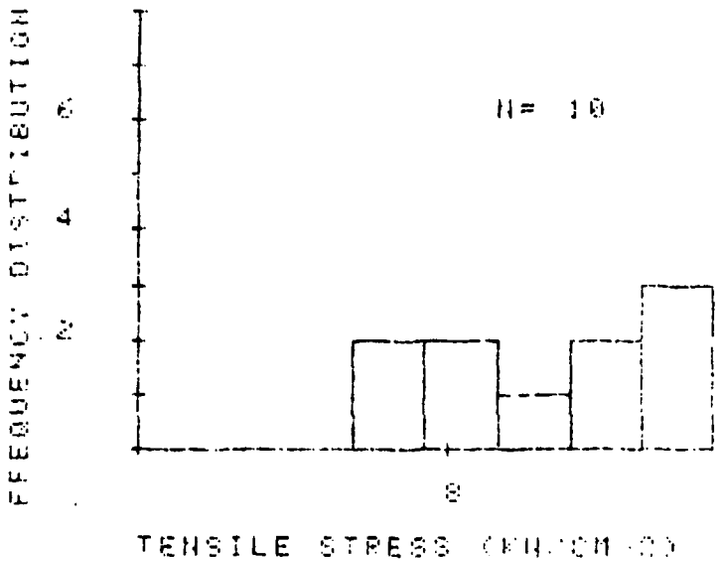

B

FIGURE 21

The frequency distribution of fracture strength for UHV deposits receiving 1.8×10^{-3} torr-sec. exposure to NH_3 before annealing and 500 torr NH_3 for 12 hrs. after annealing.
SiO_2 deposits are 3.49μ thick.

a. The fracture statistics were obtained as in Fig. 18a.
Mean fracture strength: 9.96 ± 2.26 KN/cm^2.

b. The fracture statistics were obtained as in Fig. 18b.
Mean fracture strength 8.94 ± 1.79 KN/cm^2.

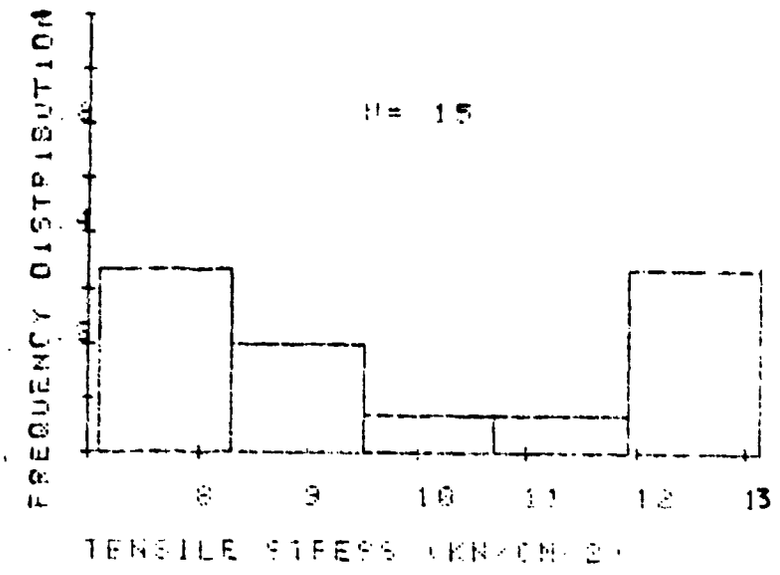
FREQUENCY DISTRIBUTION
N= 15
8
9
10
11
12
13
TENSILE STRESS (KN/CM-2)

A

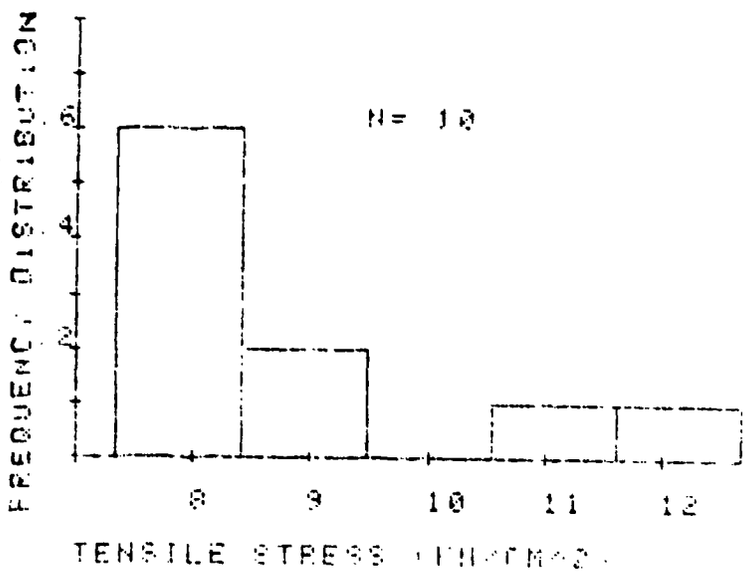
FREQUENCY DISTRIBUTION
N= 10
8
9
10
11
12
TENSILE STRESS (KN/CM-2)

B

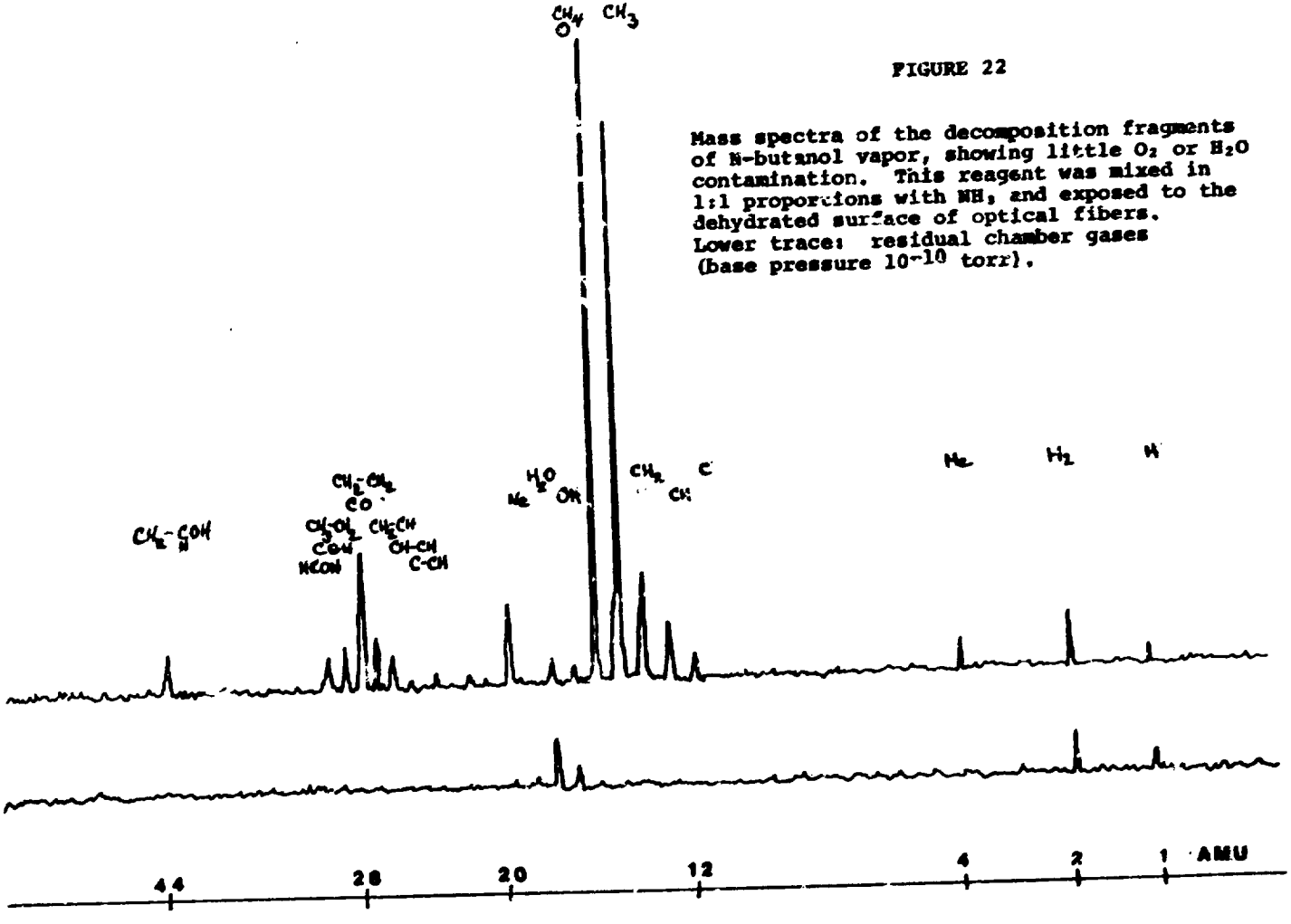

FIGURE 22

Mass spectra of the decomposition fragments of N-butanol vapor, showing little O_2 or H_2O contamination. This reagent was mixed in 1:1 proportions with NH_3 and exposed to the dehydrated surface of optical fibers. Lower trace: residual chamber gases (base pressure 10^{-10} torr).

FIGURE 23

The frequency distribution of fracture strengths for unclad optical fibers, dehydrated by heating to 400°C under 10^{-9} torr, and exposed to 3-5 torr of a 1:1 mixture of N butanol and NH_3 for 12 hrs.

a. The fracture statistics were obtained with a three point bend test. Samples were exposed to ambient gases for up to 40 min. prior to testing.
Mean fracture strength: 85.87 ± 17.48 KN/Cm^2
Compare with; 82.92 ± 23.99 KN/cm^2 (Fig. 7a)

b. Same as (a) except samples were exposed to 100% relative humidity for 24 hrs. prior to testing.
Mean fracture strength: 94.94 ± 16.12 KN/cm^2
Compare with; 100.46 ± 20.29 KN/cm^2 Fig. 7b).

FREQUENCY DISTRIBUTION
N=40
60
76
92
TENSILE STRESS (KN/CM 2)

A

FREQUENCY DISTRIBUTION
N=40
61
77
93
TENSILE STRESS (KN/CM^2)

B

APPENDIX I

Three Point Bending Analysis

The bending jig, pictured below, allows a relatively simple stress analysis for either three or four point bending tests. In the three point test both bending arms rotate about the same axis, which is coincident with the central bending edge. In this geometry the outer support pins remain at the same points on the sample during the entire test and the forces consist of normal reactions only. For analysis purposes the situation is then analogous to a beam simply supported at its ends while carrying a central concentrated load. Following Conway [72], we let R be the normal reaction at each bending arm and 2P be the normal reaction at the central support. Let y be the vertical displacement from the outer support and x the horizontal displacement from the central support to any point (x, y) and let the angle of the tangent of the beam there (measured with respect to the horizontal) be ϕ. If ϕ_o is that angle at the end supports, the vertical and horizontal forces acting at any point are respectively:

$$P = R \cos \phi_o$$

$$Q = R \sin \phi_o = P \tan \phi_o$$

Force Analysis of Three Point Bending Jig

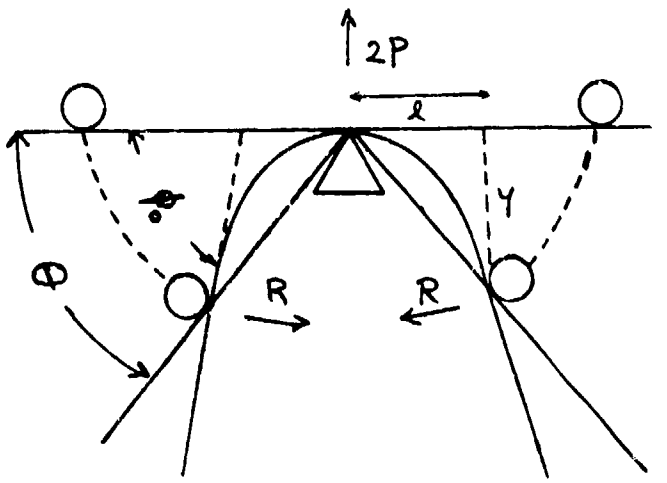

R	Normal reactions at end supports
2P	Total upward reaction at central support
2L	Length of beam between supports
I	Second moment of area of beam about neutral surface
ϕ	Angle of tangent to beam at any point (x,y), measured with respect to the horizontal
ϕ_0	Maximum angle of tangent to beam occurring at its ends
E	Young's modulus
ν	Poissons' ratio
D	Flexural Rigidity = $EI/(1-\nu^2)$
B	$\sqrt{P/D}$
θ	Angle of rotation of end supports measured with respect to the horizontal.

We have ignored the frictional component of force between the beam and its supports. The bending moment at the point (x,y) is given in terms of the curvature $-\frac{d\phi}{ds}$, where s is a segment of arc length.

$$M = D\frac{d\phi}{ds} = P(\ell - x) + P \tan \phi_o \, y \qquad (1)$$

For beams having small depth, the flexural rigidly D is taken as $EI/(1-\nu^2)$, where E is Young's modulus, I is the moment of inertia with respect to the neutral axis and ν is Poisson's ratio. The problem now breaks down to evaluating $\frac{d\phi}{ds}$, since once M is known, the tensile stress in the outer fibers of the beam is simply $\sigma = M/Z$, where Z is the section modulus. $Z = I/h/2$ for any shape beam; h is the total thickness of the beam. Differentiating equation (1) with respect to arc length -s- we obtain

$$\frac{d^2\phi}{ds^2} = -\beta^2 \cos \phi - \beta^2 \tan \phi_o \sin \phi \qquad (2)$$

with $\beta^2 = P/D$

On integrating,

$$1/2 \left(\frac{d\phi}{ds}\right)^2 = C - \beta^2 \sin \phi \cdot \beta^2 \cos \phi \tan \phi_o$$

where C is a constant of integration. The constant C is obtained from the condition that the curvature at the ends of the beam is zero and

$$\frac{d\phi}{ds} = \sqrt{2}\ \beta\ \sqrt{\sin\ \phi_o - \sin\ \phi + \tan\ \phi_o\ (\cos\ \phi - \cos\ \phi_o)} \qquad (3)$$

At the central support, which is the position of maximum stress $x = 0$, $\phi = 0$ and

$$M = D\beta\ \sqrt{2\ \tan\ \phi_o} = P(\ell + \tan\ \phi_o\ y)$$

which implies that

$$\beta = \frac{\sqrt{2\ \tan\ \phi_o}}{(\ell + \tan\ \phi_o\ y)}$$

If θ is the angle of rotation of the end supports measured with respect to the horizontal and L is the original straight line distance between the central and outer support, $\ell = L \cos\ \theta$, $y = L \sin\ \theta$ and therefore

$$M = \frac{2D\ \tan\ \phi_o}{L\ (\cos\ \theta + \tan\ \phi_o\ \sin\ \theta)} \qquad (4)$$

The shear force acting on the beam element above the central support is

$$V = \frac{dM}{dx} = -P = -\frac{2\ D\ \tan\ \phi_o}{L^2(\cos\ \theta + \tan\ \phi_o\ \sin\ \theta)^2} \qquad (5)$$

A calibration of the relationship between θ and ϕ_o was obtained photographically for the 0.0127 cm thick of molybdenum sheet and for the drawn fiber (Figures A1-1, A1-2). In cases where the variation of ϕ_o with θ did not follow a simple linear relation over the necessary range of θ values, the calibration curve was divided into a number of smaller straight line segments in order to provide linear interpolations (see Fig. A1-2). A copy of the computer program which accomplished this as well as the calculation of tensile stress is shown below. The appropriate values of Young's modulus and Poisson's ratio for the materials used are shown in the accompanying Table A-1.

Four Point Bending Analysis

The four point bending configuration (see diagram below) allows no shearing force to be impressed upon the loaded beam. Our analysis follows that of Schile and Sierakowski [73] and divides the solution into two regions of curvature. Denoting the slope (with respect to the horizontal) of the tangent by ψ, the central load by 2P, the appropriate differential equations for the bending moments are

$$M = D\frac{d\psi}{ds} = P(\ell-x) + P\tan\psi_o\,(y_{max} - y) \quad \psi_1 \leq \psi \leq \psi_o \tag{6}$$

$$M = D\frac{d\psi}{ds} = P(\ell-x) + P\tan\psi_o\,(y_{max} - y)$$

$$- P\,(\ell - \ell' - x) - P\tan\psi_1\,(y_1 - y) \quad 0 \leq \psi \leq \psi_1 \tag{7}$$

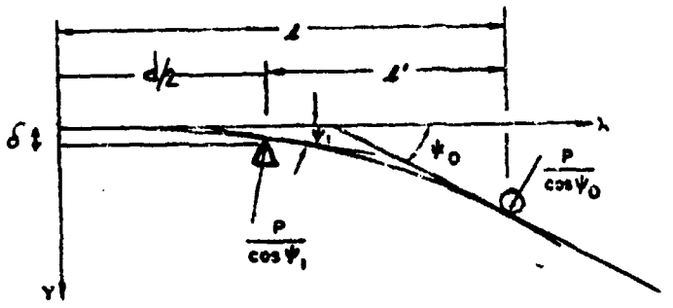

Equilibrium diagram of beam half-span
for 4 point bending.

ψ_o = the angle between the beam and the horizontal at the outer support

ψ_1 = the angle between the beam and the horizontal at the inner support

y_{max} = position of the beam measured at the point of tangency of the beam at the outer support with respect to the y coordinate at the center of the beam.

y_1 = position of the beam at the point of tangency at the inner support with respect to the y coordinate at the center of the beam.

Differentiating equations and (7) with respect to s, the arc length, and noting that

$$\frac{dy}{ds} = \sin\psi \qquad \frac{dx}{ds} = \cos\psi$$

$$\frac{d^2\psi}{ds^2} = \beta^2 (\cos\psi + \tan\psi_o \sin\psi) \qquad \psi_1 \leq \psi \leq \psi_o \tag{8}$$

$$\frac{d^2\psi}{ds^2} = \beta^2 (\tan\psi_1 - \tan\psi_o) \sin\psi \qquad 0 \leq \psi \leq \psi_1 \tag{9}$$

One integration of equations (8) and (9) yields

$$\left(\frac{d\psi}{ds}\right)^2 = 2\beta^2 (\tan\psi_o \cos\psi - \sin\psi) + C_1 \qquad \psi_1 \leq \psi \leq \psi_o$$

$$\left(\frac{d\psi}{ds}\right)^2 = 2\beta^2 (\tan\psi_o - \tan\psi_1) \cos\psi + C_2 \qquad 0 \leq \psi \leq \psi_1$$

The constants C_1 and C_2 are evaluated from the conditions

$$\left(\frac{d\psi}{ds}\right)_{\psi = \psi_o} = 0$$

$$\left(\frac{d\psi}{ds}\right)_{\psi = \psi_1 + \varepsilon} = \left(\frac{d\psi}{ds}\right)_{\psi = \psi_1 - \varepsilon} \quad \text{as} \quad \varepsilon \to 0$$

giving, $C_1 = C_2 = 0$

At the position of maximum stress $\psi = 0$, $x = 0$ and

$$M = D\beta \sqrt{2\ (\tan \psi_o - \tan \psi_1)}$$

$$= P\ (\tan \psi_o\ y_{max} + \ell' - \tan \psi_1\ y_1)$$

which implies that

$$\beta = \frac{\sqrt{2(\tan \psi_o - \tan \psi_1)}}{(\tan \psi_o\ y_{max} + \ell' - \tan \psi_1\ y_1)}$$

Referring to the Figure of the beam half-span

$$y_{max} = L \sin \theta + \delta = L \sin \theta$$

$$y_1 = \rightarrow 0$$

$$\ell' = L \cos \theta - d/2$$

and therefore

$$M = \frac{2D\ (\tan \psi_o - \tan \psi_1)}{L'(\tan \psi_o \sin \theta + \cos \theta) - d/2} \qquad (10)$$

The shear force acting on the beam element between $0 \leq \psi \leq \psi_1$ is

$$V = \frac{dM}{dx} = - P + P = 0$$

A calibration of the relationships between θ and ψ_o and between θ and ψ_1 was obtained photographically for the molybdenum sheets (Fig. A1-3). A copy of the computer program which accomplished the straight line interpolations of the calibrations as well as the calculation of tensile stress is shown below.

Corrected Tensile Stress in Outer Layers of Glass Deposits

The presence of a 3×10^{-4} to 5×10^{-4} cm layer of glass on one side of a 0.0127 cm thick substrate does not measurably alter the curvature of the substrate for a given bend angle, but it does introduce a discontinuity in the flexural rigidity D which affects the calculated stresses. To quantitate the effect, consider a substrate b cm wide and 2C cm thick on which is deposited a film of thickness Δ. Let σ_{1M} represent the maximum stress in the outer fibers of the substrate, and σ_{2M} represent the maximum stress in the outer fibers of the film. Let the plane $y = 0$ represent the neutral axis of the composite before bending, $y = y_1$ represent the interface between substrate and film, and $y = y_2$ represent the outer surface of the film. The bending moment at the cross section where the stress is maximal may be evaluated by the fact that the total moment of the internal forces Mi taken over the cross sectional area is balanced by the externally applied bending moment M.

$$M = \int_A \sigma_x \, y \, dA$$

Denoting the stress value evaluated at $y = 2C$ by σ_{1M} and the value evaluated at $y = y_2$ by σ_{2M} and noting that in the substrate $\sigma_{1x} = \sigma_{1M}\, y/C$ and in the film the stress increases linearly with y, then

$$M = \int_0^{y_1} \sigma_{1M} \frac{y^2}{C} b\, dy + \int_{y_1}^{y_2} (\sigma_{2M} - \sigma_{1M}) \frac{y^2 b\, dy}{(y_2 - y_1)}$$

$$+ \int_{y_1}^{y_2} \sigma_{1M}\, y\, b dy$$

$$= \sigma_{1M} Z_1 + b \left\{ \frac{(\sigma_{2M} - \sigma_{1M})}{3(y_2 - y_1)} (y_2^3 - y_1^3) + \frac{\sigma_{1M}}{2} (y_2^2 - y_1^2) \right\} \quad (11)$$

On the other hand, the total external moment applied is also written $M = (D_1 + D_2) \frac{d\phi}{ds}$ where D_1 is the flexural rigidity of the substrate and D_2 is the flexural rigidity of the deposited film. We have

$$D_2 = \frac{E_2}{1-\nu_2^2} \int_{y_1}^{y_2} b\, y^2\, dy = \frac{E_2 b}{1-\nu_2^2} \left(\frac{y_2^3 - y_1^3}{3}\right),$$

$$D_1 = \frac{E_1 b\, (2C)^3}{(1-\nu_1^2)12}$$

Since we also have $\sigma_{1M} Z_1 = D_1 \frac{d\phi}{ds}$, equation (11) reduces to

$$\frac{D_2}{D_1} \frac{\sigma_{1M}}{Z_1} = b \left\{ \frac{(\sigma_{2M} - \sigma_{1M})}{2 (y_2 - y_1)} (y_2^3 - y_1^3) + \frac{\sigma_{1M}}{2} (y_2^2 - y_1^2) \right\}$$

or rewritten

$$\sigma_{2M} = \sigma_{1M} \left\{ 1 + \frac{3(y_2 - y_1)}{(y_2^3 - y_1^3)} \left(\frac{D_2}{D_1} \frac{Z_1}{b} - \frac{(y_2^2 - y_1^2)}{2} \right) \right\} \qquad (12)$$

Equation 12 may be simplified to

$$\sigma_{2M} = \sigma_{1M} \left\{ 1 + \frac{\Delta}{c} \frac{E_2}{E_1} \frac{(1-\nu_1^2)}{(1-\nu_2^2)} - 3/2 \frac{\Delta [2y_1 + \Delta]}{3y_1^2 + 3y_1 \Delta + \Delta^2} \right\}$$

$$\sigma_{2M} \approx \sigma_{1M} \left\{ 1 + \frac{\Delta}{c} \frac{E_2}{E_1} \frac{(1 - \nu_2^2)}{(1 - \nu_2^2)} - \frac{\Delta}{y_1 + \Delta} \right\} \qquad (13)$$

For 0.0127 cm thick molybdenum foil, this expression can be written

$$\sigma_{2M} = \sigma_{1M} \quad 1 + 381.72 \Delta - \frac{\Delta}{.00635}$$

where Δ, the film thickness, is measured in cm. σ_{2M} amounts to a 12% increase over σ_{1M} for a 5μ deposit on a .0127 cm substrate.

TABLE A1

Elastic Modulus and Poisson Ratio for Refractory Substrate Metals and SiO_2

	E (N/cm^2)	ν
Mo	2.81×10^6	.32
SiO_2	7.40×10^6	0.16
Ni	2.13×10^6	0.31
Pd	1.195×10^6	
Ta	1.898×10^6	

FIGURE A1-1

A calibration of ϕ_o versus θ for a 0.0127 cm thick Mo sheet. The linear relation is expressed by $\phi_o = 1.10\ \theta$ for all values of θ.

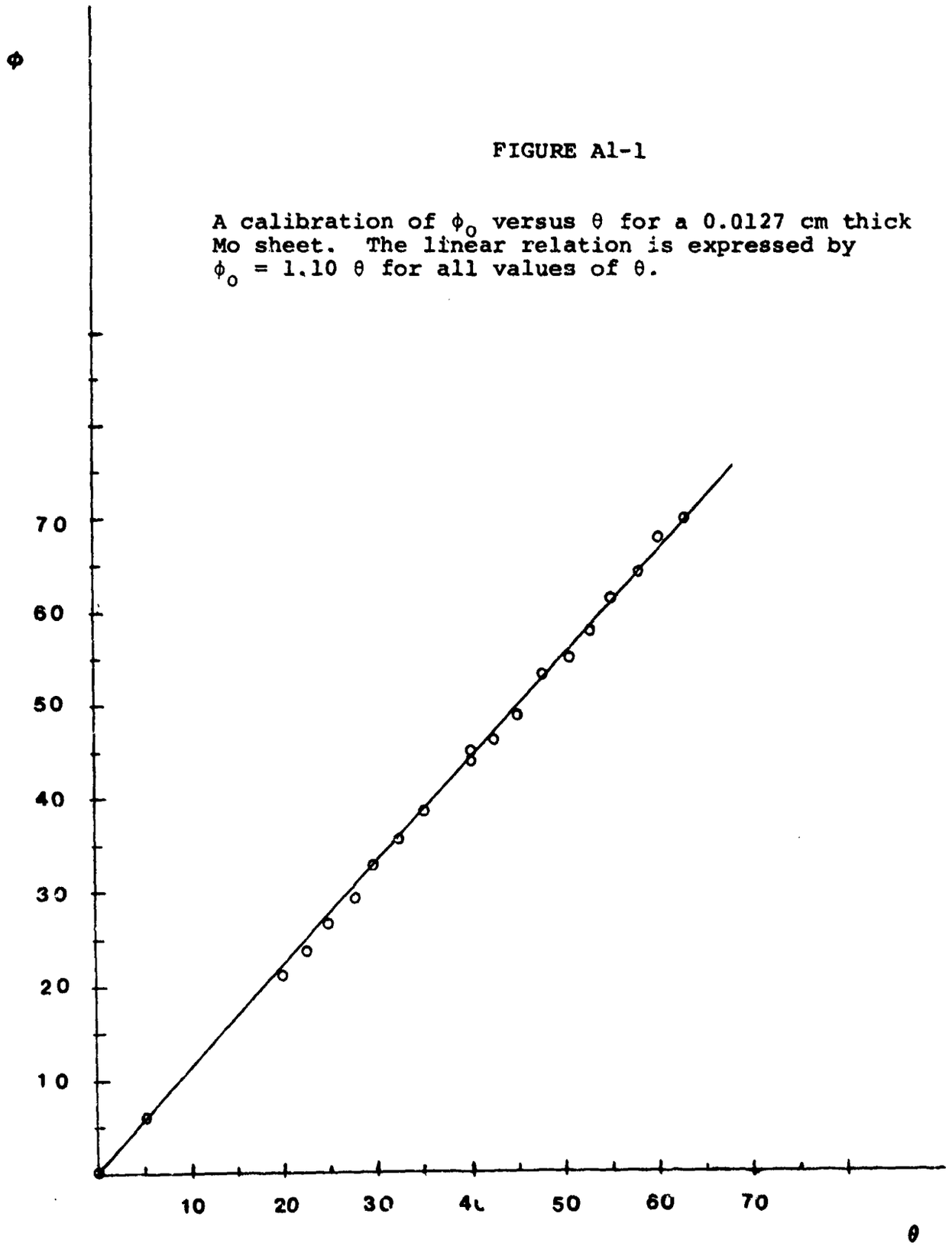

FIGURE A1-2

A calibration ϕ_o versus θ for a 200μ diameter, declad optical fiber. The three straight line segments wereused for linear interpolations in the designated ranges of θ.

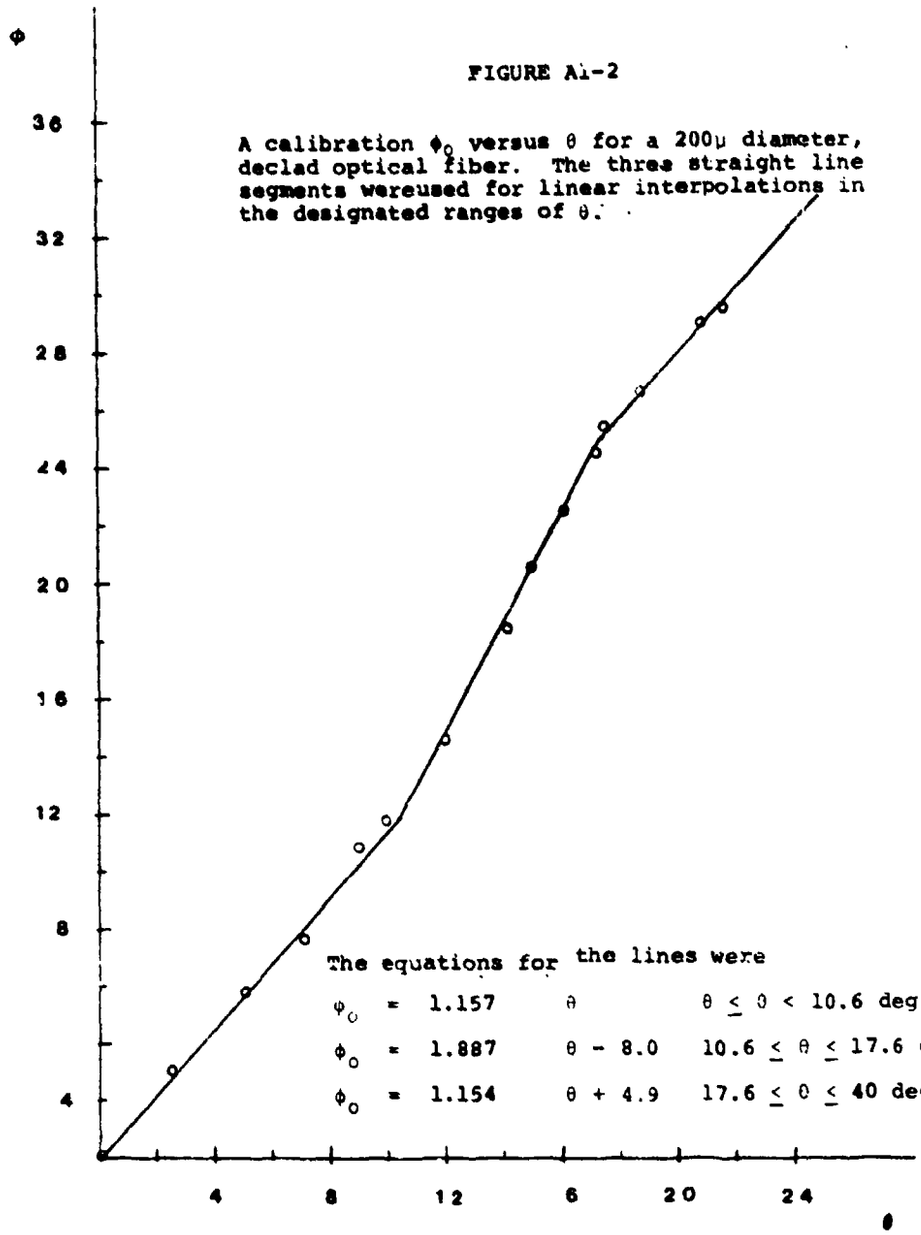

The equations for the lines were

$\phi_o = 1.157\ \theta \qquad \theta \leq \theta < 10.6$ deg.

$\phi_o = 1.887\ \theta - 8.0 \qquad 10.6 \leq \theta \leq 17.6$ deg.

$\phi_o = 1.154\ \theta + 4.9 \qquad 17.6 \leq \theta \leq 40$ deg.

1. A Listing of the Basic Program which Calculates and Plots the Tensile Strength of Glass Deposits as Determined by the Three Point Bending Configuration.

```
 10 REMS E,F'H N1,L
 11 DATA 2812300,.61214,.0127,.3
    5,.78249
 30 DISP "ENTER NO OF TEST POINT
    S,N"
 40 INPUT N
 50 DIM T1(30)
 60 L=6*H^3/12
 70 E=EA(1)/(1-N1^2)
 71 DISP "ENTER FILM THICKNESS"
 72 INPUT D6
 73 ! E=E+381 7176*D6-D6^ 00635
 80 A1=0
 90 A=0
100 FOR I=1 TO N
101 DISP "ENTER BEND ANGLE,T0"
110 INPUT T0
111 DEG
120 F0=1 1*T0
130 C=COS(T0)
140 S=SIN(T0)
150 T=TAN(F0)
160 T1(I)=2*D*T/(L*Z*(C+T*S))
161 T1(I)=T1(I)*D7
170 A=A+T1(I)
180 A2=A2+T1(I)^2
190 NEXT I
200 A=A/N
210 S1=(N*A2-A^2)/(N*(N-1))
220 S2=SQR(S1)
230 DISP "AVERAGE TENSILE STRESS
    =";A
231 PRINT "AVERAGE TENSILE STRES
    =";A
232 PRINT "STANDARD DEVIATION";S
    1
233 DISP "STANDARD DEVIATION";S2
234 PRINT "YIELD STRESS ="
235 FOR I=1 TO N
236 PRINT T1(I)
237 NEXT I
240 DISP "STANDARD DEVIATION",S2
241 DISP "ENTER FLG=SPACING IF P
    LOT DESIRED"
242 INPUT F
243 IF F<1 THEN 600
244 DIM N1(23) X(23)
250 M1=T1(1)
260 M2=T1(1)
270 FOR I=2 TO N
280 M1=MIN(T1(I),M1)
290 M2=MAX(T1(I),M2)
300 NEXT I
310 I2=F*(M2-M1)/N
320 Q=IP(N/F)
321 N1(0)=0
322 N1(Q+1)=0
330 B1=M1
340 FOR J=1 TO Q+1
350 B1=B1+I2
360 N1(J)=0
361 X(Q+2)=M2
370 FOR I=1 TO N
380 IF T1(I)<=B1 THEN 400
381 GOTO 402
400 IF T1(I)<B1-I2 THEN 402
401 N1(J)=N1(J)+1
402 NEXT I
403 NEXT J
404 FOR J=1 TO Q+1
405 N1(J)=N1(J)/N
406 X(J)=M1+I2*(J-1)
407 NEXT J
408 X(Q+1)=M2
409 X(0)=IP(M1/1000)*1000
410 GCLEAR
411 SCALE X(0)-1000,X(Q+1),-.2,.
    8
412 PEN 1
413 XAXIS 0,2000,X(0),X(Q+1)
414 YAXIS X(0),.1,0,8
417 MOVE X(0),-.2
418 LDIR 0
420 LABEL "TENSILE STRESS (KN/CM
    ^2)"
425 MOVE X(0)-750,-.1
430 LDIR 90
435 LABEL "FREQUENCY DISTRIBUTIO
    N"
436 Q1=IP((M2-M1)/2000)+1
440 FOR I=1 TO Q1
441 LDIR 0
445 A4=X(0)+2000*I
446 A3=IP(A4/1000)
449 MOVE A4,-.1
450 LABEL VAL$(A3)
460 NEXT I
461 LDIR 0
465 FOR J=.2 TO 1 STEP .2
470 MOVE X(0)-700,J
475 LABEL VAL$(J)
480 NEXT J
485 FOR J=0 TO Q+1
490 PLOT X(J),N1(J)
492 PLOT X(J+1),N1(J)
493 PLOT X(J+1),0
500 NEXT J
501 MOVE X(Q+1),N1(Q+1)
502 PLOT X(0),N1(Q+1)
505 MOVE X(Q/2),.6
506 PENUP
510 LDIR 0
515 LABEL "N= "&VAL$(N)
516 WAIT 7000
520 INPUT F
525 IF F<1 THEN 600
530 GOTO 244
600 END
```

2. **A Listing of the Basic Program which Calculates and Plots the Tensile Strength of Glass Fibers as Determined by Three Point Bending Configuration.**

```
10 READ E,P,H,N1,L
1. DATA 7400000,3.14128,.02032,
   .15,.79248
20 DISP "ENTER NO OF TEST POINT
   S";N
22 INPUT N
30 DIM T1(50)
50 I1=P*H^4/64
60 C=I1/(H/2)
70 D=E*I1/(1-N1^2)
80 A2=0
90 A=0
100 FOR I=1 TO N
101 DISP "ENTER BEND ANGLE,T0"
110 INPUT T0
111 DEG
112 IF T0<10.6 THEN 120
113 IF T0<17.6 THEN 122
114 GOTO 124
120 P0=1.1571428E*T0
121 GOTO 130
122 P0=1.386792453*T0-8
123 GOTO 130
124 P0=1.15357142857*T0+4.9
130 C=COS(T0)
140 S=SIN(T0)
150 T=TAN(P0)
160 T1(I)=2*D*T/(L*Z*(C+T*S))
170 A=A+T1(I)
180 A2=A2+T1(I)^2
190 NEXT I
200 A1=A/N
210 S1=(N*A2-A^2)/(N*(N-1))
220 S2=SQR(S1)
230 DISP "AVERAGE TENSILE STRESS
   ";A1
231 PRINT "AVERAGE TENSILE STRES
   S";A1
232 PRINT "STANDARD DEVIATION";S
   2
233 DISP "STANDARD DEVIATION";S2
234 PRINT "YIELD STRESS ="
235 FOR I=1 TO N
236 PRINT T1(I)
237 NEXT I
240 DISP "STANDARD DEVIATION";S2
241 DISP "ENTER FLG=SPACING IF P
   LOT DESIRED"
242 INPUT F
243 IF F<1 THEN 600
244 DIM N1(50),X(50)
250 M1=T1(1)
260 M2=T1(1)
270 FOR I=2 TO N
280 M1=MIN(T1(I),M1)
290 M2=MAX(T1(I),M2)
300 NEXT I
310 I2=F*(M2-M1)/N
320 Q=IP(N/F)
321 N1(0)=0
322 N1(Q+1)=0
330 B1=M1
340 FOR J=1 TO Q+1
350 S1=B1+I2
360 N1(J)=0
361 X(Q+2)=M2
370 FOR I=1 TO N
380 IF T1(I)<=B1 THEN 400
381 GOTO 402
400 IF T1(I)<B1-I2 THEN 402
401 N1(J)=N1(J)+1
402 NEXT I
403 NEXT J
404 FOR J=1 TO Q+1
405 N1(J)=N1(J)/N
406 X(J)=M1+I2*(J-1)
407 NEXT J
408 X(Q+1)=M2
409 X(0)=IP(M1/1000)*1000
410 GCLEAR
411 SCALE X(0)-16000,X(Q+1),-.2,
   .8
412 PEN 1
413 XAXIS 0,16000,X(0),X(Q+1)
414 YAXIS X(0),.1,0,.8
417 MOVE X(0),-.2
419 LDIR 0
420 LABEL "TENSILE STRESS (KN/CM
   ^2)"
425 MOVE X(0)-12000,-.1
430 LDIR 90
435 LABEL "FREQUENCY DISTRIBUTIO
   N"
436 Q1=IP((M2-M1)/16000)+1
440 FOR I=1 TO Q1
441 LDIR 0
445 A4=X(0)+16000*I
446 A3=IP(A4/1000)
449 MOVE A4,-.1
450 IF A3>99 THEN 460
451 LABEL VAL$(A3)
460 NEXT I
461 LDIR 0
465 FOR J=.2 TO 1 STEP .2
470 MOVE X(0)-8000,J
475 LABEL VAL$(J)
480 NEXT J
485 FOR J=0 TO Q+1
490 PLOT X(J),N1(J)
492 PLOT X(J+1),N1(J)
493 PLOT X(J+1),0
500 NEXT J
501 MOVE X(Q+1),N1(Q+1)
502 PLOT X(0),N1(Q+1)
505 MOVE X(Q/2),.6
510 LDIR 0
515 LABEL "N="&VAL$(N)
520 WAIT 7000
530 INPUT F
535 IF F>0 THEN 244
600 END
```

FIGURE A1-3

A calibration of ψ_0 versus θ and ψ_1 versus θ for a 0.0127 cm thick Mo sheet. The three straight line segments were used for linear interpolations of ψ_1 in the designated ranges of θ.

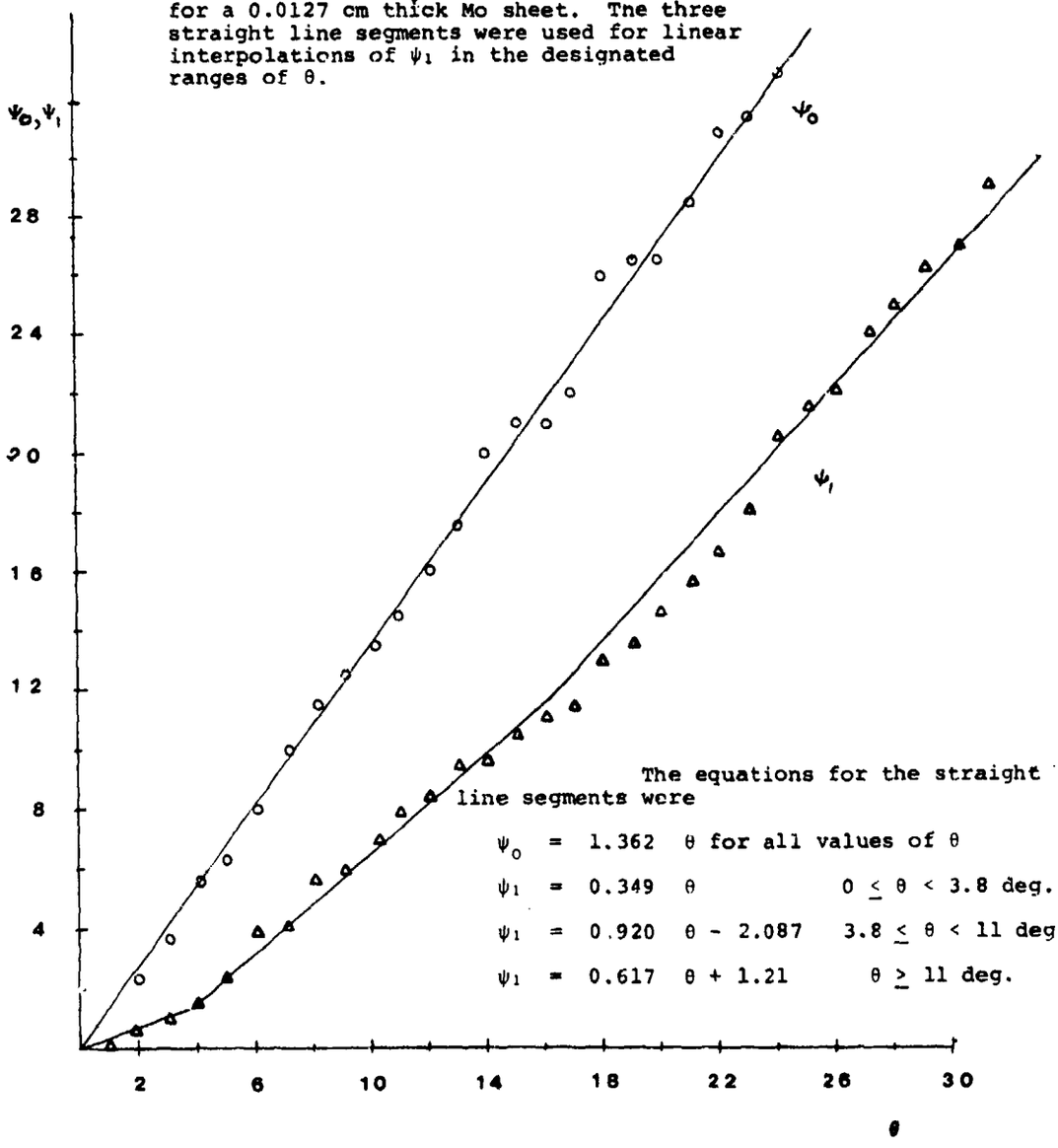

The equations for the straight line segments were

$\psi_0 = 1.362\ \theta$ for all values of θ

$\psi_1 = 0.349\ \theta$ $\quad 0 \leq \theta < 3.8$ deg.

$\psi_1 = 0.920\ \theta - 2.087$ $\quad 3.8 \leq \theta < 11$ deg.

$\psi_1 = 0.617\ \theta + 1.21$ $\quad \theta \geq 11$ deg.

3. **A Listing of the Basic Program which Calculates and Plots the Tensile Strength of Glass Deposits as Determined by the Four Point Bending Configuration.**

```
 5 !E=M0 E,P,H,N1,L,C1
 11 DATA 2612300  61714. 0127..3
    .  79242  1575
 20 DISP "ENTER NO OF TEST POINT
    S,N"
 25 INPUT N
 30 DIM T1(50)
 50 D=B*H^3/12
 60 C=I*(N^2)
 70 C=E*I1*(1-N1^2)
 71 DISP "ENTER FILM THICKNESS"
 72 INPUT D6
 73 C1=1+381.7176*D6-D6^ 00635
 80 A2=0
 90 C=0
100 FOR I=1 TO N
101 DISP "ENTER BEND ANGLE,T0"
110 INPUT T0
111 DEG
112 IF T0<3.8 THEN 120
113 IF T0<11 THEN 122
114 GOTO 124
120 P1= 348846*T0
121 GOTO 130
122 P1= 920305*T0-2.08731
123 GOTO 130
124 P1= 616667*T0+1.21
130 P0=1.3624*T0
131 C=COS(T0)
140 S=SIN(T0)
150 T=TAN(P0)
151 T2=TAN(P1)
152 T3=(T-T2)*2*D*D7
153 T4=T-T2
160 T1(I)=T3/(2*(L*S*(4+L*C-C1))
170 A=A+T1(I)
180 A2=A2+T1(I)^2
190 NEXT I
200 A1=A/N
210 S1=(N*A2-A^2)/(N*(N-1))
220 S2=SQR(S1)
230 DISP "AVERAGE TENSILE STRESS
    =";A1
231 PRINT "AVERAGE TENSILE STRES
    S=";A1
232 PRINT "STANDARD DEVIATION";S
    2
233 DISP "STANDARD DEVIATION";S2
234 PRINT "YIELD STRESS ="
235 FOR I=1 TO N
236 PRINT T1(I)
237 NEXT I
240 DISP "STANDARD DEVIATION",S2
241 DISP "ENTER FLG=SPACING IF P
    LOT DESIRED"
242 INPUT F
243 IF F<1 THEN 600
244 DIM N1(50),X(50)
250 M1=T1(1)
260 M2=T1(1)
270 FOR I=2 TO N
280 M1=MIN(T1(I),M1)
290 M2=MAX(T1(I),M2)
300 NEXT I
310 I2=F*(M2-M1)/N
320 Q=IP(N/F)
321 N1(0)=0
322 N1(Q+1)=0
330 B1=M1
340 FOR J=1 TO Q+1
350 B1=B1+I2
360 N1(J)=0
361 X(Q+2)=M2
370 FOR I=1 TO N
380 IF T1(I)=B1 THEN 400
381 GOTO 402
400 IF T1(I)<B1-I2 THEN 402
401 N1(J)=N1(J)+1
402 NEXT I
403 NEXT J
404 FOR J=1 TO Q+1
405 N1(J)=N1(J)/N
406 X(J)=M1+I2*(J-1)
407 NEXT J
408 X(Q+1)=M2
409 X(0)=IP(M1/1000)*1000
410 GCLEAR
411 SCALE X(0)-1000,X(Q+1)-X(0)+2
    00
412 PEN 1
413 XAXIS 0,1000,X(0),X(Q+1)
414 YAXIS X(0),.1,0,.8
417 MOVE X(0),-.2
418 LDIR 0
420 LABEL "TENSILE STRESS (KN/CM
    ^2)"
425 MOVE X(0)-750,-.1
430 LDIR 90
435 LABEL "FREQUENCY DISTRIBUTIO
    N"
436 Q1=IP((M2-M1)/1000)+1
440 FOR I=1 TO Q1
441 LDIR 0
445 A4=X(0)+1000*I
446 A3=IP(A4/1000)
449 MOVE A4,-.1
450 IF A3>99 THEN 460
451 LABEL VAL$(A3)
460 NEXT I
461 LDIR 0
465 FOR J=.2 TO 1 STEP .2
470 MOVE X(0)-400,J
475 LABEL VAL$(J)
480 NEXT J
485 FOR J=0 TO Q+1
490 PLOT X(J),N1(J)
492 PLOT X(J+1),N1(J)
493 PLOT X(J+1),0
500 NEXT J
501 MOVE X(Q+1),N1(Q+1)
502 PLOT X(Q),N1(Q+1)
505 MOVE X(Q/2),.6
510 LDIR 0
515 LABEL "N="&VAL$(N)
516 WAIT 7000
520 IMOVE 9000,0
525 LABEL VAL$(N)
530 INPUT F
535 IF F>0 THEN 244
600 END
```

APPENDIX II

COMPARING STRENGTH DATA OF DIFFERENT GAUGE LENGTHS/THE WEIBULL FLAW DISTRIBUTION

Following Olshansky and Maurer [47] we define a flaw distribution $n(\sigma)$ so that the number of flaws per unit length which will fail between σ and $\sigma + d\sigma$ is $n(\sigma)d\sigma$. Let $F(\sigma,L)$ be defined as the probability that a specimen of length L will fail below stress level σ, and $S(\sigma, L)$ be the analogous survival probability. Then clearly,

$$F(\sigma, L) + S(\sigma, L)) = 1 = F(\sigma, + d\sigma, 1) + S(\sigma+d\sigma,L) \qquad (1)$$

The stress level resulting in fracture is determined by the most severe flaws present in the sample. The probability that a sample will fail in the interval σ to $\sigma + d\sigma$ is a joint probability that the sample contains a flaw whose strength is in this interval and that the sample has survived to a stress level σ,

$$F(\sigma+d\sigma,L) - F(\sigma,L) = [L\, n(\sigma)\, d\sigma]\ \ S(\sigma,L) \qquad (2)$$

From Eq. (1), this can be rewritten as

$$\frac{ds(\sigma,L)}{d\sigma} = - Ln(\sigma)\ S\ (\sigma,L)$$

which has the solution

$$S(\sigma,L) = \exp\ [-\ LN(\sigma)] \tag{3}$$

where $N(\sigma)$ is the cumulative number of flaws of strength less than σ per unit length

$$N(\sigma) = \int_{o}^{\sigma} d\ \sigma^{1}\ n\ (\sigma^{1})$$

A cumulative flaw distribution, first employed by Weibull [46], was of the form

$$N(\sigma) = (\sigma/\sigma_{o})^{m} \tag{4}$$

where σ_{o} and m are empirical parameters and constant only for a well defined distribution of flaws. In general the flaws should be caused by a single mechanism or process. For a particular survival probability, samples having different gauge lengths will manifest different cumulative flaw distributions.

Let L_1, be the gauge length corresponding to a cumulative flaw distribution N_1, and L_2 the gauge length corresponding to a cumulative flaw distribution N_2. From Eq. (3) we have at a particular survival probability S,

$$L_1 N_1 = L_2 N_2$$

Substituting the same Weibull distribution for N_1 and N_2 we have finally

$$\frac{\sigma_2}{\sigma_1} = \left(\frac{L_1}{L_2}\right)^{1/m}$$

APPENDIX III

STRESS RAISERS AND CRACKS

It requires very high stress to initiate a crack in glass, but once formed, it will propagate at low stresses. The concept of stress concentration at a crack tip was first considered by Inglis [58] and somewhat later examined as an energy balance during crack propagation by Griffith [1]. For a narrow elliptical crack of length c with a semi-circular tip, radius ρ, in the edge of a thin elastic sheet to which a uniform tensile stress σ_a is applied, the tensile stress in the solid adjacent to the crack tip is given by

$$\sigma = \sigma_a \left[1 + 2 (c/\rho)^{1/2}\right] \approx 2\sigma_a (c/\rho)^{1/2} \text{ for } \rho << c \qquad (1)$$

One approach to a theory of fracture is to set this concentrated stress equal to a theoretical stress required for bond breaking or to another limit established by the flaws and homogeneous stresses in the material, and to solve for the applied stress required for fracture, σ_f.

Griffith [1] derived the same square root dependence on crack length by assuming that the change in strain energy as a crack grows is equal to the energy associated with the surface

tension in the new surface. Arguing that the the condition for the growth of a pre-existing crack under an applied stress is that the total energy should decrease as the crack length increases, he obtained the critical stress in a sheet containing and edge crack length c

$$\sigma_f = [2\ E\ \gamma/\pi\ (1 - \nu^2)\ c]^{1/2} \tag{2}$$

where γ is the surface energy, E is Young's modulus, and ν is Poisson's ratio. For plane stress, the factor $1 - \nu^2$ is replaced by unity.

The surface energy γ, invested in the newly formed surface can be related to the fracture stress involved in separating atoms in adjacent planes perpendicular to the maximum tension σ_M. The work, per cross sectional area, of an applied force required to separate the planes of the atoms completely for the equilibrium spacing d_o is as least as large as 2γ, the sum of surface energies for the two surfaces which are created. This results in the relation [74]

$$\sigma_M = (E\ \gamma/d_o)^{1/2} \tag{3}$$

Substituting this in Eq.2 gives the result that

$$\frac{\sigma_f}{\sigma_M} = [2\ d_o/\pi(1-\nu^2)\ ]^{1/2} \tag{4}$$

In as much as d_o = 1.6 Å for SiO_2, only very short elastic cracks of 1μ are needed to reduce the maximum theoretical strength σ_M by a factor of 100.

MISSION
of
Rome Air Development Center

RADC plans and executes research, development, test and selected acquisition programs in support of Command, Control Communications and Intelligence (C^3I) activities. Technical and engineering support within areas of technical competence is provided to ESD Program Officcs (POs) and other ESD elements. The principal technical mission areas are communications, electromagnetic guidance and control, surveillance of ground and aerospace objects, intelligence data collection and handling, information system technology, ionospheric propagation, solid state sciences, microwave physics and electronic reliability, maintainability and compatibility.

Printed by
United States Air Force
Hanscom AFB, Mass. 01731